Nckx30c, a *Drosophila* K^+-dependent Na^+/Ca^{2+} exchanger, regulates temperature-sensitive convulsions and age-related neurodegeneration

Al Nahian Khan Majlish[1], Sophia Bourgeois[1], Shu Hui Lye[1], Saul Landaverde[1], Emilia Cytron[1], Megan Cline[1], Harris Bolus[1], Robert N. Correll[1,2], Atulya Iyengar[1,2] & Stanislava Chtarbanova[1,2,3*]

[1] Department of Biological Sciences, The University of Alabama, Tuscaloosa, AL

[2] Center for Convergent Bioscience & Medicine, University of Alabama, Tuscaloosa, AL

[3] Alabama Life Research Institute, University of Alabama, Tuscaloosa, AL

* Corresponding author

Email: schtarbanova@ua.edu

Address: 300, Hackberry Ln, Tuscaloosa, AL-35487, USA

Phone: +1 (205)-348-1807

Keywords

Seizure, epilepsy, synaptic defects, ion transporters, calcium homeostasis, *SLC24A2*

Abstract

Calcium (Ca^{2+}) homeostasis is fundamental to neuronal physiology, including in the regulation of membrane excitability and synaptic transmission. Disruptions in the ion transporters regulating Ca^{2+} influx and efflux are clearly linked to seizure disorders and age-related neurodegenerative disease. Yet, the specific contributions of variants in genes encoding these transporters to neurological disease remain to be fully understood. *Drosophila melanogaster* has proven to be a powerful genetic model for uncovering such mechanisms, particularly through studies of mutants that display temperature-sensitive (TS) behavioral phenotypes.

In a forward genetic screen, we identified a mutant line that exhibited TS convulsions along with progressive, age-dependent neurodegeneration. We mapped the mutation to *Nckx30c*, specifically within the transmembrane ion-binding region of this K^+-dependent Na^+/Ca^{2+} exchanger. Characterization of this mutant, together with a second *Nckx30c* allele, revealed TS convulsions, impaired locomotion, a markedly shortened lifespan, neurodegeneration with age, along with structural defects at larval and adult neuromuscular junctions (NMJs). Gene expression analysis confirmed that *Nckx30c* levels were reduced in heads of *Nckx30c* loss-of-function mutants. Tissue-specific manipulation revealed that knockdown of *Nckx30c* in neurons recapitulated the TS convulsions, locomotor defects, and shortened lifespan phenotypes.

Drosophila Nckx30c is highly conserved and shares homology with mammalian *SLC24A2*, a solute carrier family 24 member whose neurological role is not yet fully elucidated. Our work establishes *Nckx30c* as an essential regulator of neuronal health and provides an *in vivo* framework for investigating the contribution of *SLC24A2* to neuronal Ca^{2+} homeostasis, seizures and age-related neurodegeneration.

Introduction

Neurodegenerative diseases (NDs) are a group of disorders characterized by the progressive loss of structure, function, and survival of neurons in the central nervous system. These conditions often lead to cognitive, motor, and behavioral impairments and are marked by common pathological features such as synaptic dysfunction and neuronal death. In 2019, it was estimated that NDs affect more than 57 million people worldwide, representing a major global health challenge. Most common examples include Alzheimer's disease (AD) and Parkinson's disease (PD) (Gadhave et al., 2024; Gao & Hong, 2008; Nichols et al., 2022; Peña-Bautista et al., 2020). One of the key features of NDs is neuronal dysfunction and cell death, which are often linked to disruption in calcium (Ca^{2+}) homeostasis, though the underlying mechanism behind this link is still being actively investigated (Sun et al., 2024). Ca^{2+} functions as a critical second messenger in neurons, translating external stimuli into precise intracellular signals that regulate a wide array of physiological processes (Bagur & Hajnóczky, 2017; Berridge, 1998; Horigane et al., 2019; Pchitskaya et al., 2018). Ca^{2+} homeostasis is crucial for regulating various functions in the nervous system, including neuronal growth and differentiation, action potential generation, and the formation of learning and memory (M. Wang et al., 2025). Disruption of Ca^{2+} dynamics not only compromises these essential processes but also contributes to neuronal hyperexcitability, which plays a central role in seizure generation (Xie et al., 2024). Seizures are episodes of sudden, abnormal, and hyper-synchronous neuronal firing that can result in transient disturbances in movement, behavior, sensation, or consciousness (Stafstrom & Carmant, 2015). This hyperexcitability is a hallmark of epileptic seizures and is often observed in neurodegenerative contexts (Amatniek et al., 2006; Gourmaud et al., 2022; Negi et al., 2023; Noebels, 2011; Tombini et al., 2021). When Ca^{2+} homeostasis is disrupted, abnormally

elevated intracellular Ca^{2+} can lower the threshold for action potential initiation and enhance repetitive firing, resulting in neuronal hyperexcitability (Mahapatra et al., 2024; Zhou et al., 2022). Thus, altered Ca^{2+} signaling serves as a shared pathological mechanism bridging seizure and ND, emphasizing the importance of studying Ca^{2+} regulation in the context of both seizure disorders and NDs. Seizures are increasingly recognized as comorbid features in several NDs, including AD. AD patients, especially those with early-onset or familial forms, exhibit an elevated risk of both clinical and subclinical seizures (Lehmann et al., 2021; Purushotham et al., 2022).

In neurons, Ca^{2+} homeostasis is regulated by a coordinated system of different ion channels, transporters and pumps (Bkaily & Jacques, 2023; Brini et al., 2014; Britzolaki et al., 2018; Gleichmann & Mattson, 2011; Mozolewski et al., 2021; Nikoletopoulou & Tavernarakis, 2012; Pizzo et al., 2012). Under resting conditions, neurons maintain a steep Ca^{2+} gradient, with intracellular Ca^{2+} concentrations being approximately 10,000 fold lower than extracellular levels (Gleichmann & Mattson, 2011). This gradient is essential for rapid Ca^{2+} signaling upon stimulation, where the influx is maintained by different voltage gated Ca^{2+} channels during depolarization (Dolphin, 2021). To restore basal levels, excess Ca^{2+} is actively extruded by plasma membrane Ca^{2+}-ATPases (PMCAs) (Krebs, 2022) and K^{+} dependent Na^{+}/Ca^{2+} exchangers (NCKXs) (A. H. Jalloul et al., 2020), the latter being a member of the most abundant Ca^{2+} extrusion protein family (Altimimi & Schnetkamp, 2007). NCKX transporters are receiving growing interest in the scientific community due to their emerging role as crucial regulators of Ca^{2+} signaling and homeostasis (Al-Khannaq & Lytton, 2022). These transporters are encoded by the *SLC24* gene family, which consists of five isoforms of the protein (NCKX1-5) found in mammals (Schnetkamp, 2013). They function with a distinct

stoichiometry of exchanging 1 Ca^{2+} and 1 K^{+} out of the cell for 4 Na^{+} in, which allows for highly efficient Ca^{2+} extrusion, particularly under physiological conditions where Na^{+} and K^{+} gradients are maintained (Jalloul et al., 2018). Among the five members of the group, NCKX2 is highly expressed in neurons, where it contributes to regulating calcium homeostasis and serves a protective role against Ca^{2+}-induced excitotoxicity (Cuomo et al., 2022; Zhang et al., 2015).

Given the evolutionary conservation of calcium signaling mechanisms, model organisms like *Drosophila melanogaster* have proven invaluable for dissecting the roles of Ca^{2+} transporters in neural function (Chorna & Hasan, 2012). The genetic tractability, well-characterized nervous system, and availability of powerful tools for cell-type-specific gene manipulation make *Drosophila* an ideal system for studying ion transporters *in vivo* (Y. Wang et al., 2018).

In *Drosophila,* two genes encode NCKX: *zydeco* and *Nckx30c*. *zydeco*, is a well-characterized example supporting the importance of Ca^{2+} extrusion in brain function that encodes a Na^{+}/Ca^{2+}, K^{+} exchanger expressed in glial cells (R. J. Winkfein et al., 2004). Disruption of *zydeco*'s function leads to impaired glial Ca^{2+} oscillations and seizures in *Drosophila* (Melom & Littleton, 2013). The *Nckx30c* has been characterized in photoreceptor cells but may have a broader role in regulating neuronal excitability and protecting against calcium-induced cytotoxicity in the brain, an area that remains underexplored. *Nckx30c* gene encodes a protein that has been described as a functional homolog of the NCKX family and is predicted to act as a K^{+}-dependent Na^{+}/Ca^{2+} exchanger involved in Ca^{2+} homeostasis with a 71% sequence identity with mammalian NCKX2 (Webel et al., 2002).

Using a forward genetic approach and screening through an N-ethyl-N-nitrosourea (ENU)-mutagenized collection of *Drosophila* mutants for the second chromosome, we identified

a novel mutant allele of *Nckx30c* that exhibits reversible TS convulsions with a point mutation that changes a threonine amino acid into a proline in the transmembrane domain of the protein. Notably, TS paralytic mutants are frequently associated with neurodegenerative phenotypes (Palladino et al., 2002), a pattern we also observed with aging for this *Nckx30c* allele. In addition to these phenotypes, *Nckx30c* mutants exhibit impaired locomotion that progressively worsens with age. Tissue specific knockdown experiments using RNA interference (RNAi) showed that *Nckx30c* function is important in neurons unlike *zydeco,* which is glial specific (Melom & Littleton, 2013). In this *Nckx30c* mutant, we also observed a morphological defect in the larval neuromuscular junction (NMJ) and loss of motor neuron branches in adult dorsal longitudinal muscle (DLM), suggesting abnormal synaptic function and neurotransmission. Based on its proposed primary function as a K^+-dependent Na^+/Ca^{2+} exchanger, *Nckx30c* may be involved in maintenance of Ca^{2+} homeostasis in the cell, and disruption of this function may result in neuronal hyperexcitability and neurodegeneration. Further investigation into *Nckx30c* and related Ca^{2+} clearance mechanisms may provide valuable insights into the molecular pathways linking Ca^{2+} dysregulation to neurodegenerative disorders and seizure susceptibility.

Materials and Methods

Drosophila stocks and maintenance

Drosophila strains were maintained at 25°C on standard cornmeal medium. The w^{1118} flies were a gift from Dr. John Yoder, University of Alabama. The ENU-mutagenized collection of *Drosophila* used in the screen including line 426 was a kind gift from Dr. Steven Robinow (University of Hawaii). The w^{1118};*Nckx30c*^{426} stock was generated by backcrossing the 426 mutant line to w^{1118} flies for at least 6 generations. The following fly lines were obtained from the Bloomington *Drosophila* Stock Center at Indiana University: y^1w^{67c23} (#6599),

w^{1118};Nckx30c^{MB06102} (#25318), *w^{1118};Nckx30c^{MB07279}* (#25268), deficiency lines for *Nckx30c – Df(2L)s1402* (#556), *Df(2L)Exel6024* (#7507), *Df(2L)ED695* (#8041), and for RNAi knockdown experiments, *elav-Gal4;UAS-dcr2* (#25750), *repo-Gal4* (#7415), four *UAS-Nckx30cRNAi* lines (#27246), (#34385), (#34386) and (#42581). An institutional ethics approval was not required for this study.

Lifespan analysis

Flies were collected three days post-eclosion and maintained at 25°C. Cohorts were transferred to fresh vials every two to three days, and daily after 20-30 days of age, to prevent older flies from adhering to the food. Each vial contained 25 flies of the same genotype. The number of surviving flies was recorded daily. Three independent survival experiments were performed for each genotype under identical conditions.

Temperature sensitive paralysis assay

For TS paralysis assay flies were collected at three days post-eclosion and aged at 25°C until they were 4-7 days old. Flies were separated by sex during the collection with 20-25 flies in each vial. The female flies were transferred to fresh vials if the food became moist or larvae were observed. For the assay flies were transferred to glass vials and placed into a glass water tank preheated to 38°C and the number of flies paralyzed or exhibiting convulsive behavior in 2 minutes was recorded. Convulsive behavior refers to the uncontrolled jerking of legs and the inability to move or fly properly (Dare et al., 2020). For the TS paralysis assay done as part of the forward genetic screen, flies were raised and aged at 25°C but transferred and kept at 18°C for 24 hours prior to TS testing.

Automated locomotion assay (video tracking)

Fly locomotion was measured using an automated open-field tracking system with heating arena following the protocol described in (Landaverde et al., 2024). Flies were placed in polyacrylate arenas set on Whatman #1 filter paper, which rested on a Peltier stage (AHP-1200CPV, TECA Corporation, Chicago, IL). Temperature within the arena was tracked using a T-type thermocouple (5SRTC-GG-T-30-36, Omega Engineering, Norwalk, CT) connected to a National Instruments NI TC-01 data acquisition card, while stage temperature was regulated by a custom LabVIEW program. Lighting was supplied by a PVC cylinder fitted with LED strips and intensity was kept at ~1000 lx with a current controller (~100 mA). Groups of four flies of the same genotype and sex were loaded into the arenas without anesthesia and recorded using a Logitech C920 webcam (30 fps). The assay protocol included baseline at 22°C (180 s), high-temperature at 36-39°C (180 s), and recovery at baseline temperature (180 s). Locomotion recordings were controlled by a LabVIEW script and analyzed in MATLAB (R2023b, Mathworks, Natick, MA) with IowaFLI Tracker to calculate distance traveled (Iyengar et al., 2012).

Immunohistochemistry

For larval NMJ analysis, wandering third instar larvae were dissected in phosphate buffered saline (1X PBS). After removing internal organs, specimens were fixed in 4% paraformaldehyde (PFA) in 1X PBS for 30 minutes on a rotating shaker. After removal of fixative solution, specimens were washed 2 times with 0.1% Triton X-100 in 1X PBS (PBS-T) for 10 minutes each, replacing with fresh PBS-T at each step. After the final wash larvae were incubated in a blocking solution of PBS-T and 4% normal goat serum (MP Biomedicals, Cat. # ICN19135680) for 1 hour. After removing the blocking solution, the larvae were incubated for another hour with 1:200 Alexa Fluor 594 goat anti-horseradish peroxidase (Jackson ImmunoResearch Cat. #123-

585-021). Incubation with the antibodies was done in dark conditions and at room temperature. After the incubation, the antibodies were removed, and the larvae were washed 3 times with PBS-T for 10 minutes each on a rotating shaker. Following the final wash, samples were mounted in ProLong™ Glass Antifade Mountant with NucBlue™ (Invitrogen, Cat. # P36981). Imaging was done using Nikon Eclipse Ti2 Laser Scanning Confocal Microscope and processed using Fiji ImageJ2 (Version: 2.16.0/1.54p). Boutons and satellite boutons were separately counted.

For dorsal longitudinal muscle (DLM) NMJ analysis, DLMs were prepared by removing the head, wings, legs and abdomen from adult thoraces, followed by fixation in 4% paraformaldehyde in 1X PBS for 30 minutes at room temperature. Thoraces were washed 4 times with 1X PBS and flash-frozen by placing the tubes with thoraces in liquid nitrogen for 20 seconds. Frozen thoraces were bisected along the midline in ice-cold 1X PBS and incubated in blocking buffer of PBS-T and 4% normal goat serum (MP Biomedicals, Cat. # ICN19135680) for at least 1 hour at 4°C, adapted from the protocol of Sidisky and Babcock (2020) (Sidisky & Babcock, 2020). Bisected hemi-thoraces were incubated with 1:200 Alexa Fluor 594 goat anti-horseradish peroxidase (Jackson ImmunoResearch, Cat. # 123-585-021) in blocking solution for 2 hours in the dark at room temperature. Following staining, samples were washed 4 times in PBS-T for 5 minutes each. Samples were mounted in Invitrogen™ ProLong™ Glass Antifade Mountant with NucBlue™ (Invitrogen, Cat. # P36981). Imaging was done using Nikon Eclipse Ti2 Laser Scanning Confocal Microscope and processed using Fiji ImageJ2 (Version: 2.16.0/1.54p).

Histology

Flies were collected upon eclosion and aged at 29°C. Severed fly heads were placed in fresh Carnoy's fixative solution (6 parts 100% ethanol, 3 parts chloroform, and 1 part glacial acetic acid) and left overnight at 4°C before exchanging into 70% ethanol the next day. Then the heads were processed into paraffin blocks using standard histological procedures following the protocol as described in Gevedon *et al*. (Gevedon et al., 2019). Head samples were paraffin embedded at the Experimental Animal Pathology Lab (EAPL) facility at the University of Wisconsin-Madison. Using a microtome (Leica Biosystems), embedded heads were sectioned at 5 μm and stained using hematoxylin and eosin (H&E). Neurodegeneration was observed on the stained midbrain sections using a light microscope (Nikon) and quantified based on neurodegeneration index as described by Cao *et al*. (Cao et al., 2013). The average of three consecutive midbrain slices were used to assign the final score of one brain sample.

Gene mutation analysis

Genomic DNA was extracted from lines *1484* (a line from the ENU mutagenized collection not exhibiting TS paralysis at 4-7 days of age), *426*, and $y^{1}w^{67c23}$ whole flies using the PureLink Genomic DNA Mini Kit (Invitrogen). Primers targeting *Nckx30c* exons (**Supplementary Table 1**) were used for amplification by PCR with Phusion® High-Fidelity DNA Polymerase (Thermo Scientific™) and DMSO, following the manufacturer's recommendations. PCR cycling conditions were as follows: initial denaturation at 98°C for 30 seconds; 35 cycles of denaturation at 98°C for 10 seconds, annealing at 65°C for 30 seconds, and extension at 72°C for 35 seconds; followed by a final extension at 72°C for 1 minute and 15 seconds. PCR product sizes were confirmed by electrophoresis on a 1% agarose gel using the GeneRuler 1 kb Plus DNA ladder (Thermo Fisher).

For cDNA analysis, total RNA was extracted from whole flies of the *426* and $y^{1}w^{67c23}$strains. cDNA synthesis was performed using the SuperScript™ IV First-Strand cDNA Synthesis Kit (Invitrogen) with a *Nckx30c*-specific primer (**Supplementary Table 1**), according to the manufacturer's instructions. PCR amplification of cDNA was carried out under the following conditions: initial denaturation at 98°C for 30 seconds; 35 cycles of denaturation at 98°C for 10 seconds and annealing/extension at 75°C for 2 minutes and 15 seconds; followed by a final extension at 75°C for 10 minutes. Sanger sequencing for both genomic and cDNA PCR products was performed by Eurofins Genomics, and sequence data were analyzed using UGENE software.

For predicting secondary protein structure organization, we used PSIPRED (Protein Analysis Workbench). Using the full-length *Drosophila Nckx30c* amino acid sequence, we ran the web server with default settings, which returns per-residue probabilities for helix (H), strand (E), and coil (C).

Gene expression analysis

Total RNA was extracted from the heads of 15-20 flies per genotype (7 day-old) using the Quick-RNA MicroPrep Kit (Zymo Research), following the manufacturer's instructions. cDNA was synthesized from 500 ng of the extracted RNA using the High-Capacity cDNA Reverse Transcription Kit (Applied Biosystems).

RT-qPCR reactions were performed using SYBR Green Master Mix (Applied Biosystems) in a 10 µL total volume. Each reaction contained 5 µL SYBR Green, 0.5 µL each of 10 µM forward and reverse primers, and nuclease-free water to make up 9 µL of reaction mix. 1 microliter of cDNA, diluted 1:10 with nuclease-free water, was added to each reaction well.

Amplification was carried out using a standard two-hour RT-qPCR protocol. The primers used for RT-qPCR reactions are listed in the **Supplementary Table 1.**

Statistical analysis

All statistical analyses were performed in GraphPad Prism v.10, except for automated locomotion data, where statistical analysis was done in MATLAB using the statistics toolkit. For each test, the "n" numbers are given in the figure legends. Lifespan (survival) curves were compared using the Log-Rank (Mantel-Cox) test. Automated locomotion data were analyzed with a Kruskal-Wallis test followed by a Bonferroni-corrected rank-sum post hoc test. For larval NMJ bouton and satellite bouton counts, mean values were assessed by one-way ANOVA with Dunnett's post-hoc test versus the control. Histology based neurodegeneration quantification was analyzed by two-way ANOVA with Tukey's multiple comparisons. For gene expression analysis, relative expression was calculated by the $2^{-\Delta\Delta CT}$ method using *Rp49* as the endogenous control and relative to w^{1118} (set to 1), and group differences were tested by one-way ANOVA with Dunnett's post-hoc test.

Results

Identification and mapping of a novel mutant exhibiting TS convulsions

To identify novel genes involved in temperature-sensitive (TS) convulsions and neurodegeneration in *Drosophila*, we performed a TS paralysis screen using a collection of 50 ENU mutants of *Drosophila* chromosome 2. Among the 50 mutant lines tested, the line designated as *426* exhibited 100% paralysis or convulsions at 38°C in 5-day-old flies (**Figure 1A**). The convulsive phenotype was only observed in homozygous, but not heterozygous *426* mutants, suggesting a recessive nature of the mutation. Heterozygous mutants were obtained by

crossing the *426* mutant with *Canton S wild type* flies. (**Figure 1B**). To map the location of the mutation on *Drosophila* chromosome 2, we performed complementation tests with a series of deficiency lines (10 deficiency lines were used and crossed with *426* mutant) based on TS convulsive behavior. The mutant line *426* failed to complement the deficiency line *Df(2L)N22-14* carrying chromosomal deletions that was located on chromosome 2L (29C1-30C9 cytological region). Using 5 additional deficiency lines, including *Df(2L)N22-14* of this region and crossing them with the mutant, we were able to identify more precisely where on chromosome 2L the TS phenotype overlapped. Thus, we mapped the TS phenotype to the left arm of chromosome 2, where the gene *Nckx30c* is located (**Figure S1**). Henceforth, *426* is referred to as $Nckx30c^{426}$.

$Nckx30c^{426}$ mutants carry a point mutation in exon 2

We performed Sanger sequencing on the $Nckx30c^{426}$ mutant, using the *1484* line (from the TS screen and not showing the TS phenotype at the age at which flies were examined) and $y^{1}w^{67c23}$ flies as controls. We sequenced the coding regions spanning all eight exons of *Nckx30c* and compared them with the reference DNA sequence. Our analysis revealed a single nucleotide substitution at position 13,179 on exon 2, where adenine (A) was replaced by cytosine (C) in the $Nckx30c^{426}$ mutant but not in the controls (**Figure 2A**). We also performed cDNA sequencing to confirm that the A to C substitution was retained in the mature mRNA and not removed through alternate splicing. Subsequent amino acid analysis showed that this mutation results in a missense change, replacing threonine (T) with proline (P) (**Figure S2A**). By using PSIPRED prediction tool for predicting helix regions in protein structure, we found that the threonine lies in the alpha helix region of the protein (**Figure S2B**). This amino acid substitution is predicted to disrupt helix structure. We used the Pfam (currently InterPro) database to analyze the mutant

amino acid sequence and found that the T to P change was in the Na^{+}/Ca^{2+} exchange domain (**Figure 2A**). Additionally, we analyzed the structure of the mutant protein using a protein modeling software (SWISS-MODEL) and compared it with the reference Nckx30c structure finding that the residue change of T to P was indeed predicted to be in the transmembrane domain. Multiple alignments of the Nckx30c protein sequence including the mutant amino acid against other *Drosophila* species and mammalian (*Homo sapiens* and *Mus musculus*) NCKX2 showed that this region is conserved among all the species (**Figure 2B**).

To further investigate the gene's function, we utilized two additional P-element insertion mutants: w^{1118};$Nckx30c^{MB07279}$, (insertion in exon 2) and w^{1118};$Nckx30c^{MB06102}$ (insertion in intron 2) (**Figure 2A**). TS paralysis assays revealed that w^{1118};$Nckx30c^{MB07279}$ but not w^{1118};$Nckx30c^{MB06102}$ mutant exhibited a convulsive phenotype similar to the $Nckx30c^{426}$ mutant. In the w^{1118};$Nckx30c^{MB07279}$ mutants, 92% of females and 88% of males exhibited the TS convulsion phenotype. In contrast, the w^{1118};$Nckx30c^{MB06102}$ mutants showed the phenotype in only 13% of females and 8% of males. (**Figure 2C**). Gene expression analysis from the heads of 7-days old males of these mutant lines demonstrated that w^{1118};$Nckx30c^{426}$ displayed significantly reduced *Nckx30c* expression compared to the w^{1118} control (P =0.0477). Additionally, w^{1118};$Nckx30c^{MB07279}$ displayed even more reduction in expression than w^{1118} (P =0.0087). In contrast, w^{1118};$Nckx30c^{MB06102}$ didn't show statistically significant differences relative to w^{1118} (**Figure 2D**). Together, these results suggest that the mutation is present in the ion transfer domain and the TS convulsion phenotype may arise from reduced *Nckx30c* expression.

***Nckx30c* mutants exhibit age-dependent neurodegeneration and shorter lifespan**

Temperature-sensitive (TS) paralytic mutants are often associated with neurodegeneration (Palladino et al., 2002). In *Drosophila*, paralytic and convulsive behavior are both phenotypes of the nervous system abnormalities, sharing some common mechanisms (Burg & Wu, 2012). A secondary histology screen using paraffin-embedded brain sections of 4 week-old *Nckx30c*^{426} mutants (n=3) and $y^{1}w^{67c23}$ (n=3) controls were tested for manifestation of neuropathology. We observed the appearance of holes considered a hallmark of neurodegeneration in mutant but not in control brains (**Figure S3**). Here, the images were obtained at the initial stages of characterizing the *Nckx30c*^{426} mutant, so quantification was not done (**Figure S3**). Given that w^{1118};*Nckx30c*^{MB07279} also exhibited TS convulsions, we further examined neurodegeneration in this mutant by comparing brain morphology between w^{1118};*Nckx30c*^{MB07279} and control w^{1118} flies at 5 and 30 days of age. Neurodegeneration was quantified in a double-blind manner using the neurodegeneration index described by Cao *et al*. (Cao et al., 2013) where higher scores indicate more severe degeneration (see Methods section for details). For 5 day-old flies, w^{1118};*Nckx30c*^{MB07279} (n=6) and w^{1118} (n=8) displayed comparable neurodegeneration indexes of 1.3 and 1.5 respectively, which were not significantly different (P =0.978). However, by 30 days, w^{1118};*Nckx30c*^{MB07279} brains (n=8) exhibited a significantly higher score of 3.5 compared to w^{1118} controls (n = 19) scoring 2.5 (P = 0.0243). This suggests that w^{1118};*Nckx30c*^{MB07279} shows age-dependent neurodegeneration **(Figure 3A)**.

We next assessed the lifespan of both homozygous w^{1118};*Nckx30c*^{MB07279} and w^{1118};*Nckx30c*^{MB06102}, as well as heterozygous w^{1118};*Nckx30c*^{MB07279}/+ and w^{1118};*Nckx30c*^{MB06102}/+ mutants and compared these flies to w^{1118} controls. In females, w^{1118};*Nckx30c*^{MB07279} (n=75) displayed significantly shorter lifespan compared to w^{1118};*Nckx30c*^{MB07279}/+ (n=75); P <0.0001 and w^{1118} (n=75); P <0.0001 where nearly all the flies died around 80 days. Whereas

w^{1118};*Nckx30c*^{MB06102} (n=74) didn't show any significant change in their lifespan compared to w^{1118};*Nckx30c*^{MB06102}/+ (n=72) and w^{1118}. Both the heterozygotes w^{1118};*Nckx30c*^{MB07279}/+ and w^{1118};*Nckx30c*^{MB06102}/+ lived longer than control w^{1118} (P =0.0191 and P =0.0289 respectively). Similarly in males, w^{1118};*Nckx30c*^{MB07279} (n=75) displayed significantly shorter lifespan compared to w^{1118};*Nckx30c*^{MB07279}/+ (n=75); P <0.0001 and w^{1118} (n=75); P <0.0001 where almost all the flies died around 70 days. However, male w^{1118};*Nckx30c*^{MB06102} (n=75) also showed significantly shorter lifespan than w^{1118};*Nckx30c*^{MB06102}/+ (n=64); P <0.0001 and w^{1118} (P <0.0001). For males, the heterozygotes didn't show any significant change in their lifespan compared to w^{1118}. These findings suggest that homozygous w^{1118};*Nckx30c*^{MB07279} mutants exhibit a significantly reduced lifespan in both males and females, whereas homozygous w^{1118};*Nckx30c*^{MB06102} mutants display a shorter lifespan only in males **(Figure 3B)**. This suggests that there might be some other internal processes in males that reduce the lifespan, as we didn't observe a significant reduction of *Nckx30c* expression in w^{1118};*Nckx30c*^{MB06102} male fly heads. It will be helpful to mention here that some isoforms of the mammalian NCKX family showed mutant phenotype but didn't reduce gene expression as shown by Jalloul and colleagues (Jalloul et al., 2016; Ali H. Jalloul et al., 2020; Robert J. Winkfein et al., 2003).

Locomotor deficits in *Nckx30c* mutants exacerbate with aging

To evaluate locomotor activity, we used an automated movement tracking system to record flies carrying different *Nckx30c* mutant alleles. Representative movement tracks at 22°C illustrate the locomotor defects in *Nckx30c* mutants compared with the w^{1118} controls. At 5 days, both w^{1118};*Nckx30c*^{426} and w^{1118};*Nckx30c*^{MB07279} mutants already showed reduced activity compared to

w^{1118} and w^{1118};*Nckx30c*^{MB06102} flies, and these defects became more severe by 30 days of age (**Figure 4A**).

Quantification of total distance traveled over a 3-minute observation period at 22°C was measured in both young (5 days old) and aged (30 day old) flies, for both sexes. At 5 days of age, female w^{1118};*Nckx30c*^{426} flies on average traveled 42.22% less than w^{1118} females, while male w^{1118};*Nckx30c*^{426} travelled 21.8% less in comparison to w^{1118} males. Path linearity, defined as the ratio of displacement to total distance over 2-second intervals, was also reduced by 12.07% in females and 8.82% in males. In comparison to w^{1118} controls, w^{1118};*Nckx30c*^{MB07279} flies displayed a similar pattern, with reductions in distance traveled of 34.62% (females) and 53.81% (males), and reductions in path linearity of 13.27% (females) and 21.25% (males). By contrast, w^{1118};*Nckx30c*^{MB06102} flies did not differ significantly from w^{1118} at this age (**Figure 4B**).

At 30 days of age, all genotypes exhibited lower locomotion than their younger counterparts. In w^{1118};*Nckx30c*^{426} flies, distance traveled was reduced by 90.6% in females and 80.4% in males, while path linearity declined by 47.27% and 33.82%, respectively, compared with w^{1118}. w^{1118};*Nckx30c*^{MB07279} flies also showed pronounced locomotor impairment, with distance traveled reduced by 76.87% (females) and 32.15% (males), and path linearity reduced by 35.66% (females) and 10.91% (males). For w^{1118};*Nckx30c*^{MB06102}, we observed a significant reduction in distance traveled only in 30 days old females (60.51%), whereas males did not differ significantly from controls. Path linearity remained unchanged in both sexes for this genotype (**Figure 4C**).

Additionally, to assess the functional consequences of different *Nckx30c* mutations, we generated compound heterozygotes of different combinations between the three alleles: w^{1118};*Nckx30c*^{426} (point mutation in exon 2), *Nckx30c*^{MB07279} (P-element insertion in exon 2), and

Nckx30c^{MB06102} (P-element insertion in intron 2) and *w*^{1118} controls. The combinations were: *w*^{1118};*Nckx30c*$^{426/+}$ (used as control), *w*^{1118};*Nckx30c*$^{426/MB07279}$, *w*^{1118};*Nckx30c*$^{426/MB06102}$ and *w*^{1118};*Nckx30c*$^{MB07279/MB06102}$. This approach allowed us to test whether different combinations of *Nckx30c* alleles differentially impact locomotor behavior. We measured the total distance traveled by each compound heterozygote at 5 and 30 days for both females and males at 22°C and 39°C. At 22°C, for 5 days old female and male *w*^{1118};*Nckx30c*$^{MB07279/MB06102}$ flies showed significantly reduced locomotion with 59.34% and 59.82% decrease in traveling distance than the control. Whereas for the other allele combinations females didn't display any significant change in their traveling distance, male *w*^{1118};*Nckx30c*$^{426/MB07279}$ and *w*^{1118};*Nckx30c*$^{426/MB06102}$ compound heterozygote flies, showed a reduction in their traveling distance by 35.46% and 15.87% respectively. However, at 30 days, none of the female groups showed any significant change in their traveling distance. Although for males, we observed a significant decrease of 56.04% in traveling distance in *w*^{1118};*Nckx30c*$^{426/MB07279}$ flies compared to the control. (**Figure S4**). However, at high temperature (39°C), at 5 days of age, female *w*^{1118};*Nckx30c*$^{426/MB07279}$ displayed an 87.5% reduction, and males, a 79.8% reduction in traveling distance compared to the control. Similarly, for 30 days, female *w*^{1118};*Nckx30c*$^{426/MB07279}$ displayed a 96.1% reduction in traveling distance, and for males, a 95.8% reduction, compared to the control. However, at 5 days, female *w*^{1118};*Nckx30c*$^{426/MB06102}$ flies showed a 5.2% reduction in traveling distance, and male *w*^{1118};*Nckx30c*$^{MB07279/MB06102}$ flies showed an 18.01% reduction in traveling distance compared to control. At 30 days, none other groups than *w*^{1118};*Nckx30c*$^{426/MB07279}$ flies displayed any significant change for both sexes (**Figure S5**). What can be inferred from these results is that the allelic interactions are highly complex in relation to locomotor behavior. At baseline temperature, the locomotor behavior is not just the functional consequence of exon 2 mutations;

the intron 2 mutation may also contribute to the phenotype when combined with the other two alleles. We also saw sex-specific differences, which might indicate a sex-dependent contribution of w^{1118};*Nckx30c*^{MB06102} in compound heterozygotes, consistent with what was observed in the w^{1118};*Nckx30c*^{MB06102} homozygous female flies but at an older age (**Figure 4C**). At high temperature, males recapitulate the baseline temperature pattern, but this time, the female w^{1118};*Nckx30c*$^{426/MB07279}$ flies also show locomotor defects. This implies that although the mutation in w^{1118};*Nckx30c*^{MB06102} is present in intron 2, the functional consequence of this allele may contribute to the locomotor defect in a heteroallelic combination with other mutant alleles.

***Nckx30c* mutants exhibit synaptic morphology defects at the larval neuromuscular junction (NMJ) and loss of motor neuron branches in adult dorsal longitudinal muscle (DLM)**

Mutations in ion channel genes that disrupt ion homeostasis can lead to morphological defects at the neuromuscular junction (NMJ), often characterized by increased neurotransmitter release and synaptic hyperexcitability (Budnik et al., 1990). We hypothesized that mutations in *Nckx30c* affect synaptic morphology at the larval NMJ. To test this, we analyzed muscle 4 of third-instar larvae, which exhibits stereotypical NMJ morphology and bouton formation. Using immunohistochemistry we quantified the bouton and satellite bouton numbers from NMJ at muscle 4 from each of the abdominal hemisegments. In w^{1118} (n=25), used as a control, we observed 15 ± 3 boutons per NMJ and no satellite boutons. These values served as a baseline for comparison with *Nckx30c* mutants NMJ. Both w^{1118};*Nckx30c*^{426} and w^{1118};*Nckx30c*^{MB07279} *had* 16 ± 2 and 18 ± 2 boutons per NMJ, respectively, and the difference was not significant. However, we detected the presence of satellite boutons in both mutants, with w^{1118};*Nckx30c*^{426} showing 3 ± 2 and w^{1118};*Nckx30c*^{MB0727} showing 4 ± 2 satellite boutons per NMJ. This represents a significant

increase compared to the absence of satellite boutons in w^{1118} larvae ($P < 0.0001$) for both mutants (**Figure 5A**). The presence of satellite boutons could be associated with abnormal neurotransmitter release, a hallmark of synaptic dysfunction (Rossetto et al., 2011).

To determine whether the structural integrity of adult neuromuscular junctions (NMJs) is affected in *Nckx30c* mutants, we characterized the motor neuron morphology in dorsal longitudinal muscles (DLMs) in young (5 days) and old (30 days) flies. Adult thoraces were dissected and stained with anti-HRP to visualize motor neuron architecture (Sidisky & Babcock, 2020). 5 day-old w^{1118} control flies displayed stereotypic highly branched motor neurons innervating the DLM fibers, while both w^{1118};*Nckx30c*^{426} and w^{1118};*Nckx30c*^{MB0727} lines exhibited reduced motor neuron branching (**Figure 5B**). By 30 days of age, these defects were exacerbated, with substantial loss of axonal branches and reduced innervation of DLM fibers. In contrast, w^{1118} flies maintained intact with elaborate motor neuron branching. These findings indicate that *Nckx30c* is required to maintain NMJ structure, and its loss leads to progressive reductions in motor neuron branching in DLMs, likely contributing to the locomotor impairments observed in *Nckx30c* mutant flies.

Neuron-specific knockdown of *Nckx30c* results in TS convulsions, locomotor defects and shortens lifespan while glial knockdown causes age-dependent locomotor decline

To determine the cell-type specificity of *Nckx30c* function underlying the observed TS convulsion phenotype, we performed targeted knockdown experiments in the nervous system. Notably, previous studies have shown that the NCKX family member *zydeco* induces TS paralysis and Ca^{2+} fluctuations when knocked down specifically in glial cells (Melom &

Littleton, 2013), prompting us to assess whether *Nckx30c* has a similar or distinct cellular requirement.

We used a *UAS-Nckx30c-RNAi* line (#27246) to reduce *Nckx30c* expression in a cell type specific manner in the nervous system. Neuronal knockdown was achieved using *elav-Gal4*;*UAS-dcr2,* and glial knockdown using *repo-Gal4*. Flies with neuronal knockdown, *elav-Gal4*;*UAS-dcr2>UAS-Nckx30c-RNAi* (n=75), showed TS convulsion, with 42 out of 75 (56%) of female and 60 out of 75 (80%) of male flies displaying the phenotype. In contrast, the glial knockdown, *repo-Gal4>UAS-Nckx30c-RNAi* (n=75), flies didn't show any convulsion for either sex (**Figure 6A**). To validate the specificity of the convulsive phenotype, we tested three additional *UAS-Nckx30c-RNAi* lines (#34385, #34386, and #42581). All RNAi lines targeting neurons using *elav-Gal4;UAS-dcr2* recapitulated the TS convulsive phenotype. With *UAS-Nckx30c-RNAi* (#34385), 23 out of 75 (~31%) females and 24 out of 75 (32%) males; *UAS-Nckx30c-RNAi* (#34386), 42 out of 75 (~56%) females and 55 out of 75 (74%) males and with *UAS-Nckx30c-RNAi* (#42581), 33 out of 75 (~44%) females and 58 out of 75 (78%) males displayed the TS phenotype. For knockdown experiments, the genetic controls were: *elav-Gal4;UAS-dcr2>+* (driver control), *repo-Gal4>+* (driver control), and *UAS-Nckx30c-RNAi>+* (RNAi control) (**Figure 6A**).

For our subsequent *UAS-Nckx30c-RNAi* experiments, we used line #27246. To verify knockdown efficiency, we performed RT-qPCR and found that *elav-Gal4*;*UAS-dcr2>UAS-Nckx30c-RNAi* flies showed a reduction in *Nckx30c* expression in whole heads compared to the control *elav-Gal4;UAS-dcr2>+*, confirming knockdown was achieved. We also observed a reduction in *Nckx30c* expression in *repo-Gal4>UAS-Nckx30c-RNAi* flies compared to their

control *repo-Gal4*>+ , however, this reduction was to a lower extent than the neuronal knockdown (**Figure S6**).

We next examined locomotor activity in *Nckx30c* knockdown flies using the automated video tracking system at 22°C. Assays were performed on both 5 day and 30 day-old flies, in males and females, across *elav-Gal4*;*UAS-dcr2*>*UAS-Nckx30c-RNAi* and *repo-Gal4*>*UAS-Nckx30c-RNAi*, compared to the RNAi control *UAS-Nckx30c-RNAi*>+ (where *UAS-Nckx30c-RNAi* crossed with w^{1118}). Representative locomotor tracks illustrate reduced movement in *elav-Gal4*;*UAS-dcr2*>*UAS-Nckx30c-RNAi* flies at 5 days, and in both *elav-Gal4*;*UAS-dcr2*>*UAS-Nckx30c-RNAi* and *repo-Gal4*>*UAS-Nckx30c-RNAi* flies at 30 days, relative to controls (**Figure 6B**).

At 5 days, female *elav-Gal4*;*UAS-dcr2*>*UAS-Nckx30c-RNAi* (n=60) flies showed a marked locomotor defect, with an 84.78% reduction in total distance traveled and a 39.98% reduction in path linearity compared with control *UAS-Nckx30c-RNAi*>+ (n=56). Female *repo-Gal4*>*UAS-Nckx30c-RNAi* (n=52) flies exhibited a 34.27% reduction in distance traveled and a decrease in path linearity, but these changes were not statistically significant. In males, *elav-Gal4*;*UAS-dcr2*>*UAS-Nckx30c-RNAi* (n=40) flies displayed a 30.47% reduction in distance traveled, whereas *repo-Gal4*>*UAS-Nckx30c-RNAi* (n=47) males showed only an 18.71% reduction. For path linearity, *elav-Gal4*;*UAS-dcr2*>*UAS-Nckx30c-RNAi* males exhibited a non-significant decrease of 8.05%, while *repo-Gal4*>*UAS-Nckx30c-RNAi* males showed an 11% increase relative to the control *UAS-Nckx30c-RNAi*>+ (n=48).

At 30 days, locomotor activity was reduced across all genotypes. In females, neither *elav-Gal4*;*UAS-dcr2*>*UAS-Nckx30c-RNAi* (n=32) nor *repo-Gal4*>*UAS-Nckx30c-RNAi* (n=52) flies

displayed significant reductions in distance traveled or path linearity compared with controls. In contrast, males *repo-Gal4>UAS-Nckx30c-RNAi* (n=44) flies exhibited almost a 99% reduction in distance traveled and a 40.62% decrease in path linearity, while *elav-Gal4*;*UAS-dcr2>UAS-Nckx30c-RNAi* (n=44) males did not differ significantly from controls (**Figure 6C**).

Finally, we assessed the effect of *Nckx30c* knockdown on lifespan using *elav-Gal4;UAS-dcr2>UAS-Nckx30c-RNAi* and *repo-Gal4>UAS-Nckx30c-RNAi.* In females, neuronal knockdown *elav-Gal4;UAS-dcr2>UAS-Nckx30c-RNAi* (n=67) significantly reduced lifespan compared to both controls *elav-Gal4;UAS-dcr2>+* (n=71); P <0.0001 and *UAS-Nckx30c-RNAi>+* (n=70); P <0.0001, and almost all the flies died before 80 days. Glial knockdown flies, *repo-Gal4>UAS-Nckx30c-RNAi* (n=84) also showed reduced lifespan compared to control *repo-Gal4>+* (n=82); P =0.0086 and *UAS-Nckx30c-RNAi>+* (n=70); P <0.0001, where almost all the flies died before 90 days. Furthermore, neuronal knockdown flies *elav-Gal4;UAS-dcr2>UAS-Nckx30c-RNAi* showed significantly shorter lifespan compared to glial knockdown flies *repo-Gal4>UAS-Nckx30c-RNAi* (P =0.0006). Similarly, *elav-Gal4;UAS-dcr2>UAS-Nckx30c-RNAi* (n=83) males displayed significantly reduced lifespan compared to both controls *elav-Gal4;UAS-dcr2>+* (n=90); P =0.0260 and *UAS-Nckx30c-RNAi>+* (n=86); P <0.0001. The difference in lifespan was not as pronounced as observed in the females. *repo-Gal4>UAS-Nckx30c-RNAi* (n=92) didn't display any significant change in their lifespan compared to control *repo-Gal4>+* (n=102); but they showed significantly shorter lifespan than *UAS-Nckx30c-RNAi>+* (n=86); P =0.0004. Compared to glial knockdown flies, *repo-Gal4>UAS-Nckx30c-RNAi*, neuronal knockdown flies, *elav-Gal4;UAS-dcr2>UAS-Nckx30c-RNAi,* showed significantly shorter lifespan; P =0.0168. From the observed results, we found that for both females and males, neuron-specific *Nckx30c* knock down resulted in the shortest lifespan among all the genotypes

examined (**Figure 6D**). These findings collectively indicate that *Nckx30c* plays a role in neuronal function, where its knockdown is sufficient to induce TS convulsions, early-onset locomotor defects, and a significantly shortened lifespan, while glial knockdown contributes to locomotor decline at later ages and also reduces lifespan relative to controls.

Discussion

This study identifies *Nckx30c* as a potential regulator of neuronal excitability, synaptic integrity, and proper function of the nervous system in *Drosophila melanogaster*. Through a combination of forward genetics and gene functional characterization, we identified a loss-of-function *Nckx30c* mutant that displays temperature-sensitive convulsions, age-dependent neurodegeneration, progressive locomotor decline, and shortened lifespan. In *426* mutant flies, we mapped the mutation to exon 2 of the *Nckx30c* gene within its conserved Na^+/Ca^{2+} exchange domain. This highlights what is likely to be a functional disruption of the K^+-dependent Na^+/Ca^{2+} exchanger encoded by *Nckx30c*.

Temperature sensitive (TS) paralysis in *Drosophila* has been traditionally utilized to identify genes that are crucial for neuronal excitability, including ion channels and Ca^{2+} regulators, revealing key proteins in ion conductance (Ganetzky & Wu, 1986; D. T. Suzuki et al., 1971). A major advantage of forward TS screens is that they allow unbiased identification of genes required for neuronal signaling simply by observing behavioral paralysis, without prior knowledge of the underlying gene or protein. This screening technique is also useful in identifying mutations that display convulsion or seizure like behavior (P. Wang et al., 2004). The TS convulsive phenotype observed in *Nckx30c*^{426} mutants aligns with previous reports that associate TS paralysis with impaired neuronal excitability and ion homeostasis (Palladino et al., 2002; David T Suzuki et al., 1971). Given its proposed role as a Ca^{2+} exchanger, our findings

suggest that *Nckx30c* may contribute to maintaining neuronal Ca^{2+} homeostasis under high temperature stress. Interestingly, the P-element insertion mutant *Nckx30c*^{MB07279}, which disrupts the same exon as the point mutant, also displayed TS convulsion and reduced gene expression, whereas *Nckx30c*^{MB06102}, with an insertion in an intron, did not. This suggests that mutations directly affecting coding regions or regulatory exons of *Nckx30c* are necessary to elicit the phenotype, potentially due to a more severe loss of function.

A hallmark feature of many TS mutants is their association with progressive neurodegeneration (Palladino et al., 2002). Consistently, both *Nckx30c*^{426} and *Nckx30c*^{MB07279} mutants developed age-dependent brain neuropathology, accompanied by a significantly shortened lifespan. These results reinforce the emerging view that ionic imbalances, particularly calcium dysregulation, are a key contributor to neuronal vulnerability with age (Gleichmann & Mattson, 2011; Stolwijk et al., 2016). The observation that neurodegeneration becomes more pronounced at older ages may reflect cumulative mitochondrial dysfunction and excitotoxic stress, possibly arising from sustained calcium imbalance.

The locomotor analysis using compound heterozygotes revealed that only *Nckx30c*$^{426/MB07279}$ exhibited a significant defect in movement, particularly under high-temperature conditions, while other allele combinations did not. This finding suggests that the two exon 2 mutations, *Nckx30c*^{426} (point mutation) and *Nckx30c*^{MB07279} (P-element insertion), represent loss-of-function alleles that fail to complement one another. Their combined effect likely disrupts *Nckx30c* function below the threshold required to maintain normal neuronal activity and locomotor behavior. In contrast, we found that heterozygotes involving *Nckx30c*^{MB06102} (intronic P-element insertion) exhibited behavior comparable to *w*^{1118};*Nckx30c*$^{426/+}$ heterozygotes, indicating that this allele may have minimal or no functional

impact on gene expression. The absence of locomotor impairment in these combinations highlights the importance of exon integrity for *Nckx30c* function. The locomotor defect observed in w^{1118};*Nckx30c*$^{426/MB07279}$ flies was most noticeable under high-temperature stress, and the severity increased with age. These findings suggest that *Nckx30c* plays a role in maintaining neuronal integrity and locomotor function under conditions of physiological stress.

Over the years, *Drosophila* has enabled the identification and functional characterization of numerous genes and pathways involved in neuroprotection and neurodegeneration, many of which are conserved in humans (Bilen & Bonini, 2005). Additionally, studies of the *Drosophila* larval neuromuscular junction (NMJ), a synaptic link between the motor nerve's terminal end and a muscle, have provided key insights into the mechanisms regulating synapse development, growth, and neurotransmission. Functionally, these glutamatergic synapses resemble mammalian central synapses and undergo structural remodeling in response to neuronal activity (Collins & DiAntonio, 2007; Gramates & Budnik, 1999; Juel, 2012). The larval NMJ is the classic model system for studying ion channels (such as K^+, Ca^{2+}), mutants for which often show altered bouton number and synaptic overgrowth with satellite boutons (Lee & Wu, 2010; Menon et al., 2013). The adult dorsal longitudinal muscle (DLM) NMJ, an indirect flight-muscle synapse essential for escape, provides a complementary aging model. Its stereotyped innervation permits precise quantification of motor-neuron branching and connectivity (Allen et al., 2006). In *mayday* and *shibire* fly mutants, DLM fibers show progressive, age-dependent loss of motor neuron branching (Beramendi et al., 2007; Sidisky & Babcock, 2020; Sidisky et al., 2021). Studying NMJ integrity is essential for identifying molecular factors underlying age-related synaptic decline and neurodegeneration (Pratt et al., 2021). Our larval NMJ analysis revealed a significant synaptic abnormality in *Nckx30c* mutants with the appearance of satellite boutons.

This feature is often associated with elevated synaptic activity and altered neurotransmission (Budnik et al., 1990; Rossetto et al., 2011), suggesting that loss of *Nckx30c* disrupts synaptic structure and function, possibly due to persistent Ca^{2+} elevation in presynaptic terminals. Our analysis of DLM neuromuscular junctions provided additional evidence that *Nckx30c* plays a role in maintaining synaptic integrity throughout adulthood. The early reduction in motor neuron branching observed in both $Nckx30c^{426}$ and $Nckx30c^{MB07279}$ mutants, which becomes more pronounced with age, suggests that *Nckx30c* is required not only at early development but also for the long-term stability of NMJs. This progressive denervation is consistent with the locomotor impairments seen in mutant flies and could represent a possible link between disrupted Ca^{2+} extrusion and synaptic maintenance (Vonhoff & Keshishian, 2017). Similar age-dependent NMJ degeneration has been reported in other models of neuronal dysfunction (Sidisky & Babcock, 2020), further supporting the idea that Ca^{2+} homeostasis is essential for preserving motor neuron integrity. Thus, *Nckx30c* may function as a neuroprotective factor, with its loss predisposing flies to both structural synaptic decline and associated behavioral deficits.

Tissue-specific RNAi experiments demonstrated that *Nckx30c* is required in neurons for the temperature-sensitive (TS) convulsion phenotype, as this phenotype was observed only with neuronal knockdown and not with glial knockdown. Locomotor behavior analyses revealed that at a young age (5 days), defects were restricted to flies with neuronal knockdown. However, at an older age (30 days), glial knockdown flies also exhibited locomotor impairments. Lifespan assays further showed that neuronal knockdown resulted in the shortest lifespan, while glial knockdown also led to a significantly reduced lifespan compared to both glial and RNAi controls. The age-dependent locomotor defects and reduced lifespan associated with glial knockdown suggest that *Nckx30c* function in glial cells becomes increasingly important with

age, thereby contributing to long-term neuronal health. Notably, the other NCKX family member *zydeco,* whose TS phenotype is glia-dependent (Melom & Littleton, 2013), suggests that *Nckx30c* and *zydeco* serve distinct cellular roles in TS convulsions, but may share overlapping functions related to glial contributions in aging.

To investigate whether disruption of *Nckx30c* affects the expression of other genes involved in calcium homeostasis, we assessed the mRNA levels of *MCU* (Mitochondrial Calcium Uniporter), involved in Ca^{2+} transport into the mitochondria (Choi et al., 2017) and *PMCA* (Plasma Membrane Calcium ATPase) which plays a role in Ca^{2+} extrusion (Erhardt et al., 2021), in 7 days-old male heads of all the *Nckx30c* mutants investigated in this study, but did not observe any significant changes compared to the control strain (**Figure S7**). This suggests that the phenotypes observed at 7 days of age in male flies are linked to *Nckx30c* dysfunction rather than secondary alterations in other Ca^{2+} transport mechanisms. However, we did not check gene expression at an older age (30 days) when there could have been a compensatory effect at later time points. Also, we cannot exclude that such changes occur in discrete cells or subtypes of cells in the nervous system. Future experiments could address this by using *in-situ* hybridization or immunostaining to visualize and quantify mRNA and/or protein corresponding to these genes in dissected brains of mutants and compare them to controls. It is also possible that the reduced longevity, locomotor defects, and neurodegeneration associated with *Nckx30c* disruption may be the result of mitochondrial damage due to Ca^{2+} overload or oxidative stress. While *Drosophila* mitochondria are capable of undergoing permeability transition (von Stockum et al., 2011) they are resistant to Ca^{2+} overload (Chaudhuri et al., 2016). In mammalian cells, the *PPIF* gene (encoding Cyclophilin D) is a critical regulator of permeability transition (Baines et al., 2005) that is inhibited by cyclosporin A. While its

putative *Drosophila* homolog, Cyclophilin 1 (encoded by *Cyp1*), is insensitive to cyclosporin A (von Stockum et al., 2011), knockdown of *Cyp1* does inhibit permeability transition in cultured *Drosophila* S2R+ cells (Chaudhuri et al., 2016). Additionally, deletion of *Cyp1* is protective against oxidative stress and has been shown to improve lifespan and locomotor defects in a *Drosophila DJ-1β* mutant line that is used as a model of Parkinson's disease (Kim et al., 2018). Thus, mechanistic insight may be gained by future studies designed to examine whether *Cyp1* deletion could similarly recover the defects associated with *Nckx30c* disruption.

Looking ahead, several experiments could extend our mechanistic understanding. Electrophysiological recordings from *Nckx30c* mutants would allow direct assessment of whether altered Ca^{2+} extrusion changes spontaneous neuronal firing, synaptic activity, or responses to electroconvulsive stimulation. Genetic rescue approaches also hold promise: reintroducing *Nckx30c* itself or expressing K^+ leak channels could help determine whether the observed mutant phenotypes arise solely from Ca^{2+} accumulation or whether altered K^+ handling also contributes. Overexpressing Ca^{2+} leak channels could work as an attempt to rescue the mutant phenotype. Finally, exploring genetic interactions between *Nckx30c* mutants and models of neurodegeneration such as AD models could provide insight into how Ca^{2+} dysregulation intersects with amyloid-driven pathology. While the connection between NCKX family members and human NDs has not been extensively investigated, the human *Nckx30c* ortholog *SLC24A2* (NCKX2) is suggested to play a role in neuronal Ca^{2+} extrusion and has been implicated in NDs, more recently, in AD. One study based on genome-wide association using whole-genome sequencing of apolipoprotein E ε4 (APOE ε4) carriers identified *SLC24A2* as one of twelve loci significantly associated with AD risk. Here 500 individual participated in the study with 331 of them being AD patients (Park et al., 2021). Another study reported an elevated levels of

NCKX2 phospho-peptides in the serum of AD patients compared to controls, although it remains uncertain whether this increase reflects NCKX2 release from defective neurons or changes in the expression of NCKX2 and post-translational modifications (Florentinus-Mefailoski et al., 2021). While this study only examined n= 24 individuals among whom 12 were AD patients, these findings suggest that disruption of NCKX2 function may contribute to neurodegenerative vulnerability. Testing if defective *Nckx30c* intensifies phenotypes would support the idea that defective ionic balance is an upstream vulnerability factor in amyloid-mediated disease.

Together, these future directions will not only clarify the neuroprotective role of *Nckx30c* but also establish its broader relevance to seizure susceptibility and neurodegenerative diseases.

Conclusion

This study provides novel insights into the role of the *Drosophila* gene *Nckx30c*, a member of the NCKX family of K^+-dependent Na^+/Ca^{2+} exchangers, in regulating neuronal excitability, synaptic integrity, and organismal health. Through a forward genetic screen, a novel mutant allele (*Nckx30c*^{426}) was identified. This mutant exhibited temperature-sensitive convulsions, age-dependent neurodegeneration, and locomotor dysfunction. Analysis of additional alleles including *Nckx30c*^{MB07279}, revealed that mutations disrupting exon 2 are particularly deleterious, emphasizing the importance of this region for ion exchanger function.

Phenotypic characterization across flies from young and old cohorts established a consistent pattern of dysfunction, where the mutant phenotype gained severity with age. Mutants displayed behavioral abnormalities at increased temperature, reduced lifespan, progressive neurodegeneration, and structural synaptic defects at both larval and adult neuromuscular junctions. Specifically, the presence of satellite boutons at larval NMJs and progressive branch

loss in adult DLM NMJs revealed that *Nckx30c* may have a role in maintaining synaptic stability throughout life. Tissue-specific knockdown experiments further demonstrated that neuronal *Nckx30c* is essential for preventing temperature sensitive convulsions, early onset of locomotor defect and maintaining lifespan, while glial knockdown contributes to age-dependent locomotor decline.

Together, our findings establish *Nckx30c* as an important regulator of Ca^{2+}-dependent neuronal processes in *Drosophila melanogaster*. By linking impaired Ca^{2+} extrusion to seizure susceptibility, synaptic abnormalities, and neurodegeneration, this work highlights a unifying mechanism through which ionic imbalance can trigger both acute and progressive neural dysfunction. This work broadens our understanding of the NCKX family by moving beyond the well-studied glial exchanger *zydeco* and uncovering *Nckx30c*, a counterpart that functions at an early age in neurons and exerts effects in glia, particularly at older ages.

The broader implications of this study are twofold. First, it reinforces the concept that Ca^{2+} dysregulation is a central mechanism connecting seizures and neurodegenerative diseases. Second, it positions *Nckx30c* as a valuable genetic model for exploring how disruptions in Ca^{2+} transport contribute to neurodegenerative disorders and epileptic seizures. By integrating genetic, behavioral, and structural approaches, this study lays the foundation for future electrophysiological, and disease-interaction studies that will further define the molecular pathways linking Ca^{2+} homeostasis, synaptic health, and neuronal survival.

In conclusion, the work presented here advances our understanding of Ca^{2+} regulation in the nervous system by establishing *Nckx30c* as a key factor in neuronal excitability and synaptic maintenance. It also provides a framework for future research into the role of NCKX exchangers

in neurodegenerative disease and seizure susceptibility, thereby contributing to the broader goal of uncovering mechanisms that safeguard neuronal function across the lifespan.

Acknowledgements

We thank Dr. Barry Ganetzky in whom laboratory this work started originally; Dr. Steven Robinow for providing the collection of ENU-mutagenized stocks used in the genetic screen; Luke Chandler for help with the forward genetic screen; Katy Marotto for help with histology, Dr. Kim Lackey at the Optical Analysis Facility at the University of Alabama for assistance with confocal microscopy. We are grateful to all our colleagues of the Ganetzky joint lab meeting for advice and helpful discussions about the project.

Funding

ANKM was supported by the University of Alabama graduate school. This work was supported by start-up funds from the University of Alabama to SC and AI, and a NIH grant R61 NS126693 to AI.

Disclosure of interest

The authors report no conflict of interest.

Authors contributions

SC conceptualized the study with input from AI and ANKM; ANKM, SB, SHL, SL, EC, MC, SC and HB performed experiments; ANKM, SB, SHL, SL, AI and SC analyzed data. ANKM wrote the original draft. RNC, AI and SC contributed to manuscript writing, review and editing.

Figure legends

Figure 1: Phenotypic characterization of a novel mutant 426 exhibiting temperature sensitive convulsions.

(A) TS paralysis screen of 50 ENU-mutagenized chromosome 2 lines 5-day-old flies from each line were placed in a 38°C water bath, and the percentage of flies showing paralysis or convulsion within 5 min was calculated. Lines showing > 0% paralysis or convulsion are presented by the graph bars. **(B)** Representative image of the TS paralysis assay at 90 seconds shows convulsive behavior in homozygous *426* mutants compared to heterozygous control (*426* mutant crossed with *Canton S*). **(C)** Complementation tests using deficiency lines. Mutant *426* failed to complement *Df(2L)N22-14* and showed TS convulsions. **(D)** Complementation tests using additional deficiency lines refined the candidate region. Here, controls are heterozygotes obtained by crossing each deficiency line to w^{1118}. Numbers inside the bars represent "n"-numbers (n=50).

Figure 2: Molecular characterization of the *Nckx30c* mutant.

(A) Schematic of the *Nckx30c* gene structure and associated mutations. The *426* mutant carries a point mutation (A to C) in exon 2, affecting a conserved region within the Na^+/Ca^{2+} exchange domain. The location of two additional P-element insertions (*MB07279* (exon 2)) and (*MB06102* (intron 2), are shown. **(B)** The predicted protein structure of $Nckx30c^{426}$ showing the mutation located in the transmembrane region. The inset (magnified region) highlights the location of the mutation. The affected region (residue 423) is evolutionarily conserved across different *Drosophila* species (10 species) and mammalian NCKX2 (*Homo sapiens* and *Mus musculus*), as

shown by the amino acid sequence alignment of Nckx30c. Here, threonine (T) is replaced by proline (P) in the mutant. **(C)** TS paralysis assay of the P-element insertion alleles w^{1118};*Nckx30c*^{MB07279} and w^{1118};*Nckx30c*^{MB06102} of both females and males compared against control w^{1118}. Numbers inside the bars represent "n"-numbers (n=25). **(D)** RT-qPCR analysis of relative expression of *Nckx30c* gene in w^{1118};*Nckx30*^{426}, w^{1118};*Nckx30c*^{MB07279} and w^{1118};*Nckx30c*^{MB06102}, compared to w^{1118} controls. The data presented here were calculated using the $2^{-\Delta\Delta CT}$ method. Data were normalized to *Rp49* gene as an endogenous control and w^{1118} as the control strain. The bar graphs show mean ± SEM; the symbols over each mutant genotype bar indicate statistical comparison against w^{1118}. Statistics: one-way ANOVA with Dunnett's post hoc test; $*P \leq 0.05$, $**P \leq 0.01$, *ns* = not significant. All the specific P values are reported in the **Supplementary dataset file.**

Figure 3: *Nckx30c* mutants exhibit age-dependent neurodegeneration and shorter lifespan. **(A)** Left panel: representative 5-µm paraffin sections at approximately midbrain of w^{1118} and w^{1118};*Nckx30c*^{MB07279}. Arrowheads indicate holes in the brain indicative of neurodegeneration. Right panel: neurodegeneration index of young (5d) and old (30d) w^{1118};*Nckx30c*^{MB07279} mutants and w^{1118} controls. Scale bar represents 250 µm. Quantification of neurodegeneration in fly brains done based on the neurodegeneration index scale from 0-5 as in Cao *et al*. (Cao et al., 2013). Values shown are mean ± SEM; two-way ANOVA with Tukey's multiple comparison test; $*P < 0.05$, *ns* = non-significant. **(B)** Lifespan curves for flies of the indicated genotypes maintained at 25°C. Numbers in parentheses indicate sample size. Log-Rank (Mantel-Cox); $*P \leq 0.05$, $****P \leq 0.0001$, *ns* = not significant. All the specific P values are reported in the **Supplementary dataset file**.

Figure 4: Automated video tracking of locomotor activity in *Nckx30c* mutants.

(A) Representative tracks of four male flies from the respective genotype (Temperature: 22°C). Left panel: 5 days-old flies, right panel: 30 days-old flies. **(B, C)** Distance traveled and path linearity at 22°C in females and males flies at 5 and 30 days were measured. Each set of box plots represents each genotype. Numbers in parentheses represent sample size. Statistics: Kruskal Wallis non-parametric ANOVA (Bonferroni-corrected rank-sum post hoc test). Data from each mutant genotype were compared against w^{1118} to generate statistical significance, represented by the symbols over each box. $^{**}P \leq 0.01$, $^{***}P \leq 0.001$, *ns* = not significant. All the specific P values are reported in the **Supplementary dataset file**.

Figure 5: *Nckx30c* mutants show larval and adult (DLM) NMJ defects.

(A) Left panel: Representative confocal images of larval NMJs at muscle 4 stained with Anti-HRP. w^{1118};*Nckx30c*^{426} and w^{1118};*Nckx30c*^{MB07279} compared with w^{1118}. White arrowheads indicate satellite boutons at synaptic termini. Right panel: Quantification of bouton numbers and satellite bouton numbers shown by the graph. Numbers in bar represent number of NMJs analyzed. Scale bar:10 µm. Each genotype was compared against w^{1118}. Statistical significance was determined by one-way ANOVA with Dunnett's post-hoc test; $^{****}P \leq 0.0001$, *ns* = not significant. **(B)** Representative confocal images of DLM NMJs labeled with Anti-HRP at 60x. Flies collected at 5 days and 30 days of age for each genotype. For each genotype and age group, n=15-20 thoraces were dissected and stained. Scale bar: 50 µm. The green dotted line marks the boundaries of a single muscle fiber. Specific P values are reported in the **Supplementary dataset file**.

Figure 6: Knockdown of *Nckx30c* in neurons and glia differentially affects behavioral phenotypes and lifespan.

(A) TS paralysis assay of *Nckx30c* knocked down in neurons (*elav-Gal4;UAS-dcr2>UAS-Nckx30c-RNAi*) and glia (*repo-Gal4>UAS-Nckx30c-RNAi*). Four different *Nckx30c* RNAi lines are used (#27246, #34385, #34386, and #42581). Numbers in each bar represent sample size. (**B**) Representative tracks of four male flies from the respective knockdown genotypes (Temperature: 22°C). top panel: 5 days-old flies, bottom panel: 30 days-old flies. **(C)** Distance traveled and path linearity was measured at 22°C in female and male flies at 5- and 30 days of age, respectively. Each set of box plots represents each genotype. Numbers in parentheses represent sample size. Statistics: Kruskal Wallis non-parametric ANOVA (Bonferroni-corrected rank-sum post hoc test). Symbols over each box represent statistical significance compared to control *UAS-Nckx30c-RNAi>+*. *$P \leq 0.05$, **$P \leq 0.01$, ***$P \leq 0.001$, *ns* = not significant. **(D)** Lifespan curves for flies of the indicated genotypes maintained at 25°C. Numbers in parentheses indicate sample size. Log-Rank (Mantel-Cox); *$P \leq 0.05$, **$P \leq 0.01$, ***$P \leq 0.001$, ****$P \leq 0.0001$, *ns* = not significant. P values are reported in the **Supplementary dataset file.**

Supplemental figure legends

Figure S1: Deficiency mapping of *Nckx30c.*

Schematic of overlapping deficiency lines used for mapping. The overlapping region includes the *Nckx30c* gene locus. *426* mutants fail to complement deficiency lines indicated by the pink boxes, implicating cytological region 30C6–30C7 (black dotted line). The phenotype was scored using a yes/no method where a genotype showing a paralytic phenotype was scored as yes, and the one not showing a phenotype was scored as no.

Figure S2: cDNA sequencing and alignment of *Nckx30c* and predicted helix region.

(A) cDNA sequence of *Nckx30c* was acquired from database (Flybase.org) and then it was compared with the cDNA sequences from control y^1w^{67c23} and mutant $Nckx30c^{426}$. The alignment against cDNA from the database shows a change in adenine (A) to cytosine (C) at nucleotide position 1126 in the mutant $Nckx30c^{426}$, indicated by the black dotted line. Subsequent translated amino acid sequence alignment shows a change in threonine (T) to proline (P) at residue position 376. **(B)** Predicted helix region (tool: PSIPRED) shows that the T might be present in the helix region (marked by a green box). Yellow represents the beta strand, pink represents the alpha helix and gray represents irregular coils.

Figure S3: *Nckx30c* mutants exhibit neurodegeneration.

Representative 5-µm paraffin sections at approximately midbrain of 26-day old control y^1w^{67c23} (n=3) and $Nckx30c^{426}$ (n=3) mutant flies. The presence of holes (arrowheads) is indicative of neurodegeneration. Images were taken at 20x magnification using a light microscope.

Figure S4: Locomotor behavior analysis of *Nckx30c* compound heterozygotes at 22°C.

(A) Representative tracks of four male flies from the respective genotype (Temperature: 22°C). Top panel: 5 days old flies, bottom panel: 30 days old flies. **(B)** Automated open-field behavior tracking to measure distance traveled at 22°C in females and males flies at 5 and 30 days of age, respectively. Each set of box plots represents each genotype. Numbers in parentheses represent sample size. Statistics: Kruskal Wallis non-parametric ANOVA (Bonferroni-corrected rank-sum post hoc test). Data from each mutant genotype were compared against w^{1118};$Nckx30c^{426/+}$ to generate statistical significance, represented by the symbols over each box. *$P \leq 0.05$, ***$P \leq 0.001$, *ns* = not significant. *P* values are reported in the **Supplementary dataset file.**

Figure S5: Locomotor behavior analysis of *Nckx30c* compound heterozygotes at 39°C.

(A) Representative tracks of four male flies from the respective genotype (Temperature: 39°C). Top panel: 5 days-old flies, bottom panel: 30 days-old flies. **(B)** Automated open-field behavior tracking to measure distance traveled at 39°C in female and male flies at 5- and 30 days of age, respectively. Each set of box plots represents each genotype. Numbers in parentheses represent sample size. Statistics: Kruskal Wallis non-parametric ANOVA (Bonferroni-corrected rank-sum post hoc test). Data from each mutant genotype were compared against w^{1118};$Nckx30c^{426/+}$ to generate statistical significance, represented by the symbols over each box. **$P \leq 0.01$, ***$P \leq 0.001$, *ns* = not significant. *P* values are reported in the **Supplementary dataset file.**

Figure S6: RT-qPCR analysis for the verification of *Nckx30c* knockdown.

RT-qPCR analysis of relative expression of *Nckx30c* gene in *elav-Gal4;UAS-dcr2>+*, *elav-Gal4;UAS-dcr2>UAS-Nckx30c-RNAi*, *repo-Gal4>+* and *repo-Gal4>UAS-Nckx30c-RNAi*. Here, *elav-Gal4;UAS-dcr2>UAS-Nckx30c-RNAi* shows lower expression of *Nckx30c* than the control

elav-Gal4;UAS-dcr2>+. It is also showing lower expression than *repo-Gal4>UAS-Nckx30c-RNAi.* While the difference between glial knockdown *repo-Gal4>UAS-Nckx30c-RNAi* and control *repo-Gal4>+* is not as much as the latter one. Independent experiment number: n=1. Gene expression data were normalized to the *Rp49* gene as an endogenous control.

Figure S7: RT-qPCR analysis of calcium regulating genes.

RT-qPCR analysis of relative expression of *MCU and PMCA* genes, respectively, in heads of w^{1118}*;Nckx30*^{426}, w^{1118}*;Nckx30c*^{MB07279} *and* w^{1118}*;Nckx30c*^{MB06102} flies compared to w^{1118} controls. All samples were from 7-days old male flies. Independent experiment number: n=6. Mean ± SEM; one-way ANOVA with Dunnett's post-hoc test; *ns* = not significant. All gene expression data were normalized to *Rp49* gene and shown as relative to w^{1118}. P values are reported in the **Supplementary dataset file.**

Supplementary Table 1: List of primers used in this study.

Supplementary dataset file: P-values from statistical analysis in all figures.

References

Al-Khannaq, M., & Lytton, J. (2022). Regulation of K+-dependent Na+/Ca2+-exchangers (NCKX). *International journal of molecular sciences*, *24*(1), 598.

Allen, M. J., Godenschwege, T. A., Tanouye, M. A., & Phelan, P. (2006). Making an escape: development and function of the Drosophila giant fibre system. *Semin Cell Dev Biol*, *17*(1), 31-41. https://doi.org/10.1016/j.semcdb.2005.11.011

Altimimi, H. F., & Schnetkamp, P. P. (2007). Na+/Ca2+-K+ exchangers (NCKX): functional properties and physiological roles. *Channels (Austin)*, *1*(2), 62-69. https://doi.org/10.4161/chan.4366

Amatniek, J. C., Hauser, W. A., DelCastillo-Castaneda, C., Jacobs, D. M., Marder, K., Bell, K., Albert, M., Brandt, J., & Stern, Y. (2006). Incidence and Predictors of Seizures in Patients with Alzheimer's Disease. *Epilepsia*, *47*(5), 867-872. https://doi.org/https://doi.org/10.1111/j.1528-1167.2006.00554.x

Bagur, R., & Hajnóczky, G. (2017). Intracellular Ca(2+) Sensing: Its Role in Calcium Homeostasis and Signaling. *Mol Cell*, *66*(6), 780-788. https://doi.org/10.1016/j.molcel.2017.05.028

Baines, C. P., Kaiser, R. A., Purcell, N. H., Blair, N. S., Osinska, H., Hambleton, M. A., Brunskill, E. W., Sayen, M. R., Gottlieb, R. A., Dorn, G. W., Robbins, J., & Molkentin, J. D. (2005). Loss of cyclophilin D reveals a critical role for mitochondrial permeability transition in cell death. *Nature*, *434*(7033), 658-662. https://doi.org/10.1038/nature03434

Beramendi, A., Peron, S., Casanova, G., Reggiani, C., & Cantera, R. (2007). Neuromuscular junction in abdominal muscles of Drosophila melanogaster during adulthood and aging. *J Comp Neurol*, *501*(4), 498-508. https://doi.org/10.1002/cne.21253

Berridge, M. J. (1998). Neuronal Calcium Signaling. *Neuron*, *21*(1), 13-26. https://doi.org/10.1016/S0896-6273(00)80510-3

Bilen, J., & Bonini, N. M. (2005). Drosophila as a model for human neurodegenerative disease. *Annu Rev Genet*, *39*, 153-171. https://doi.org/10.1146/annurev.genet.39.110304.095804

Bkaily, G., & Jacques, D. (2023). Calcium Homeostasis, Transporters, and Blockers in Health and Diseases of the Cardiovascular System. *Int J Mol Sci*, *24*(10). https://doi.org/10.3390/ijms24108803

Brini, M., Calì, T., Ottolini, D., & Carafoli, E. (2014). Neuronal calcium signaling: function and dysfunction. *Cell Mol Life Sci*, *71*(15), 2787-2814. https://doi.org/10.1007/s00018-013-1550-7

Britzolaki, A., Saurine, J., Flaherty, E., Thelen, C., & Pitychoutis, P. M. (2018). The SERCA2: A Gatekeeper of Neuronal Calcium Homeostasis in the Brain. *Cell Mol Neurobiol*, *38*(5), 981-994. https://doi.org/10.1007/s10571-018-0583-8

Budnik, V., Zhong, Y., & Wu, C. F. (1990). Morphological plasticity of motor axons in Drosophila mutants with altered excitability. *J Neurosci*, *10*(11), 3754-3768. https://doi.org/10.1523/jneurosci.10-11-03754.1990

Burg, M. G., & Wu, C. F. (2012). Mechanical and temperature stressor-induced seizure-and-paralysis behaviors in Drosophila bang-sensitive mutants. *J Neurogenet*, *26*(2), 189-197. https://doi.org/10.3109/01677063.2012.690011

Cao, Y., Chtarbanova, S., Petersen, A. J., & Ganetzky, B. (2013). Dnr1 mutations cause neurodegeneration in Drosophila by activating the innate immune response in the brain. *Proceedings of the National Academy of Sciences*, *110*(19), E1752-E1760. https://doi.org/doi:10.1073/pnas.1306220110

Chaudhuri, D., Artiga, D. J., Abiria, S. A., & Clapham, D. E. (2016). Mitochondrial calcium uniporter regulator 1 (MCUR1) regulates the calcium threshold for the mitochondrial permeability transition. *Proc Natl Acad Sci U S A*, *113*(13), E1872-1880. https://doi.org/10.1073/pnas.1602264113

Choi, S., Quan, X., Bang, S., Yoo, H., Kim, J., Park, J., Park, K. S., & Chung, J. (2017). Mitochondrial calcium uniporter in Drosophila transfers calcium between the endoplasmic reticulum and mitochondria in oxidative stress-induced cell death. *J Biol Chem*, *292*(35), 14473-14485. https://doi.org/10.1074/jbc.M116.765578

Chorna, T., & Hasan, G. (2012). The genetics of calcium signaling in Drosophila melanogaster. *Biochimica et Biophysica Acta (BBA) - General Subjects*, *1820*(8), 1269-1282. https://doi.org/https://doi.org/10.1016/j.bbagen.2011.11.002

Collins, C. A., & DiAntonio, A. (2007). Synaptic development: insights from Drosophila. *Curr Opin Neurobiol*, *17*(1), 35-42. https://doi.org/10.1016/j.conb.2007.01.001

Cuomo, O., Sirabella, R., Boscia, F., Casamassa, A., Lytton, J., Annunziato, L., & Pignataro, G. (2022). K(+)-Dependent Na(+)/Ca(2+) Exchanger Isoform 2, Nckx2, Takes Part in the Neuroprotection Elicited by Ischemic Preconditioning in Brain Ischemia. *Int J Mol Sci*, *23*(13). https://doi.org/10.3390/ijms23137128

Dare, S. S., Merlo, E., Rodriguez Curt, J., Ekanem, P. E., Hu, N., & Berni, J. (2020). Drosophila para (bss) Flies as a Screening Model for Traditional Medicine: Anticonvulsant Effects of Annona senegalensis. *Front Neurol*, *11*, 606919. https://doi.org/10.3389/fneur.2020.606919

Dolphin, A. C. (2021). Functions of Presynaptic Voltage-gated Calcium Channels. *Function (Oxf)*, *2*(1), zqaa027. https://doi.org/10.1093/function/zqaa027

Erhardt, B., Marcora, M. S., Frenkel, L., Bochicchio, P. A., Bodin, D. H., Silva, B. A., Farías, M. I., Allo, M., Höcht, C., Ferrari, C. C., Pitossi, F. J., & Leal, M. C. (2021). Plasma membrane calcium ATPase downregulation in dopaminergic neurons alters cellular physiology and motor behaviour in Drosophila melanogaster. *Eur J Neurosci*, *54*(6), 5915-5931. https://doi.org/10.1111/ejn.15401

Florentinus-Mefailoski, A., Bowden, P., Scheltens, P., Killestein, J., Teunissen, C., & Marshall, J. G. (2021). The plasma peptides of Alzheimer's disease. *Clin Proteomics*, *18*(1), 17. https://doi.org/10.1186/s12014-021-09320-2

Gadhave, D. G., Sugandhi, V. V., Jha, S. K., Nangare, S. N., Gupta, G., Singh, S. K., Dua, K., Cho, H., Hansbro, P. M., & Paudel, K. R. (2024). Neurodegenerative disorders: Mechanisms of degeneration and therapeutic approaches with their clinical relevance. *Ageing Res Rev*, *99*, 102357. https://doi.org/10.1016/j.arr.2024.102357

Ganetzky, B., & Wu, C. F. (1986). Neurogenetics of membrane excitability in Drosophila. *Annu Rev Genet*, *20*, 13-44. https://doi.org/10.1146/annurev.ge.20.120186.000305

Gao, H. M., & Hong, J. S. (2008). Why neurodegenerative diseases are progressive: uncontrolled inflammation drives disease progression. *Trends Immunol*, *29*(8), 357-365. https://doi.org/10.1016/j.it.2008.05.002

Gevedon, O., Bolus, H., Lye, S. H., Schmitz, K., Fuentes-González, J., Hatchell, K., Bley, L., Pienaar, J., Loewen, C., & Chtarbanova, S. (2019). In Vivo Forward Genetic Screen to Identify Novel Neuroprotective Genes in Drosophila melanogaster. *J Vis Exp*(149). https://doi.org/10.3791/59720

Gleichmann, M., & Mattson, M. P. (2011). Neuronal calcium homeostasis and dysregulation. *Antioxidants & redox signaling*, *14*(7), 1261-1273.

Gourmaud, S., Stewart, D. A., Irwin, D. J., Roberts, N., Barbour, A. J., Eberwine, G., O'Brien, W. T., Vassar, R., Talos, D. M., & Jensen, F. E. (2022). The role of mTORC1 activation in seizure-induced exacerbation of Alzheimer's disease. *Brain*, *145*(1), 324-339. https://doi.org/10.1093/brain/awab268

Gramates, L. S., & Budnik, V. (1999). Assembly and maturation of the Drosophila larval neuromuscular junction. *Int Rev Neurobiol*, *43*, 93-117. https://doi.org/10.1016/s0074-7742(08)60542-5

Horigane, S.-i., Ozawa, Y., Yamada, H., & Takemoto-Kimura, S. (2019). Calcium signalling: a key regulator of neuronal migration. *The Journal of Biochemistry*, *165*(5), 401-409. https://doi.org/10.1093/jb/mvz012

Iyengar, A., Imoehl, J., Ueda, A., Nirschl, J., & Wu, C. F. (2012). Automated quantification of locomotion, social interaction, and mate preference in Drosophila mutants. *J Neurogenet*, *26*(3-4), 306-316. https://doi.org/10.3109/01677063.2012.729626

Jalloul, A. H., Rogasevskaia, T. P., Szerencsei, R. T., & Schnetkamp, P. P. M. (2016). A Functional Study of Mutations in K+-dependent Na+-Ca2+ Exchangers Associated with Amelogenesis Imperfecta and Non-syndromic Oculocutaneous Albinism*. *Journal of Biological Chemistry*, *291*(25), 13113-13123. https://doi.org/https://doi.org/10.1074/jbc.M116.728824

Jalloul, A. H., Szerencsei, R. T., Rogasevskaia, T. P., & Schnetkamp, P. P. M. (2018). SLC24A Family (K+-Dependent Na+-Ca2+ Exchanger, NCKX). In S. Choi (Ed.), *Encyclopedia of Signaling Molecules* (pp. 4994-5002). Springer International Publishing. https://doi.org/10.1007/978-3-319-67199-4_101860

Jalloul, A. H., Szerencsei, R. T., Rogasevskaia, T. P., & Schnetkamp, P. P. M. (2020). Structure-function relationships of K(+)-dependent Na(+)/Ca(2+) exchangers (NCKX). *Cell Calcium*, *86*, 102153. https://doi.org/10.1016/j.ceca.2019.102153

Jalloul, A. H., Szerencsei, R. T., Rogasevskaia, T. P., & Schnetkamp, P. P. M. (2020). Structure-function relationships of K+-dependent Na+/Ca2+ exchangers (NCKX). *Cell Calcium*, *86*, 102153. https://doi.org/https://doi.org/10.1016/j.ceca.2019.102153

Juel, V. C. (2012). Evaluation of neuromuscular junction disorders in the electromyography laboratory. *Neurol Clin*, *30*(2), 621-639. https://doi.org/10.1016/j.ncl.2011.12.012

Kim, E. Y., Kang, K. H., & Koh, H. (2018). Cyclophilin 1 (Cyp1) mutation ameliorates oxidative stress-induced defects in a Drosophila DJ-1 null mutant. *Biochem Biophys Res Commun*, *505*(3), 823-829. https://doi.org/10.1016/j.bbrc.2018.10.014

Krebs, J. (2022). Structure, Function and Regulation of the Plasma Membrane Calcium Pump in Health and Disease. *Int J Mol Sci*, *23*(3). https://doi.org/10.3390/ijms23031027

Landaverde, S., Sleep, M., Lacoste, A., Tan, S., Schuback, R., Reiter, L. T., & Iyengar, A. (2024). Glial expression of Drosophila UBE3A causes spontaneous seizures that can be modulated by 5-HT signaling. *Neurobiology of Disease*, *200*, 106651. https://doi.org/https://doi.org/10.1016/j.nbd.2024.106651

Lee, J., & Wu, C. F. (2010). Orchestration of stepwise synaptic growth by K+ and Ca2+ channels in Drosophila. *J Neurosci*, *30*(47), 15821-15833. https://doi.org/10.1523/jneurosci.3448-10.2010

Lehmann, L., Lo, A., Knox, K. M., & Barker-Haliski, M. (2021). Alzheimer's Disease and Epilepsy: A Perspective on the Opportunities for Overlapping Therapeutic Innovation. *Neurochem Res*, *46*(8), 1895-1912. https://doi.org/10.1007/s11064-021-03332-y

Mahapatra, C., Thakkar, R., & Kumar, R. (2024). Modulatory Impact of Oxidative Stress on Action Potentials in Pathophysiological States: A Comprehensive Review. *Antioxidants (Basel)*, *13*(10). https://doi.org/10.3390/antiox13101172

Melom, J. E., & Littleton, J. T. (2013). Mutation of a NCKX Eliminates Glial Microdomain Calcium Oscillations and Enhances Seizure Susceptibility. *The Journal of Neuroscience*, *33*(3), 1169-1178. https://doi.org/10.1523/jneurosci.3920-12.2013

Menon, K. P., Carrillo, R. A., & Zinn, K. (2013). Development and plasticity of the Drosophila larval neuromuscular junction. *Wiley Interdiscip Rev Dev Biol*, *2*(5), 647-670. https://doi.org/10.1002/wdev.108

Mozolewski, P., Jeziorek, M., Schuster, C. M., Bading, H., Frost, B., & Dobrowolski, R. (2021). The role of nuclear Ca2+ in maintaining neuronal homeostasis and brain health. *Journal of Cell Science*, *134*(8). https://doi.org/10.1242/jcs.254904

Negi, D., Granak, S., Shorter, S., O'Leary, V. B., Rektor, I., & Ovsepian, S. V. (2023). Molecular Biomarkers of Neuronal Injury in Epilepsy Shared with Neurodegenerative Diseases. *Neurotherapeutics*, *20*(3), 767-778. https://doi.org/10.1007/s13311-023-01355-7

Nichols, E., Steinmetz, J. D., Vollset, S. E., Fukutaki, K., Chalek, J., Abd-Allah, F., Abdoli, A., Abualhasan, A., Abu-Gharbieh, E., Akram, T. T., Al Hamad, H., Alahdab, F., Alanezi, F. M., Alipour, V., Almustanyir, S., Amu, H., Ansari, I., Arabloo, J., Ashraf, T., Astell-Burt, T., Ayano, G., Ayuso-Mateos, J. L., Baig, A. A., Barnett, A., Barrow, A., Baune, B. T., Béjot, Y., Bezabhe, W. M. M., Bezabih, Y. M., Bhagavathula, A. S., Bhaskar, S., Bhattacharyya, K., Bijani, A., Biswas, A., Bolla, S. R., Boloor, A., Brayne, C., Brenner, H., Burkart, K., Burns, R. A., Cámera, L. A., Cao, C., Carvalho, F., Castro-de-Araujo, L. F. S., Catalá-López, F., Cerin, E., Chavan, P. P., Cherbuin, N., Chu, D.-T., Costa, V. M., Couto, R. A. S., Dadras, O., Dai, X., Dandona, L., Dandona, R., De la Cruz-Góngora, V., Dhamnetiya, D., Dias da Silva, D., Diaz, D., Douiri, A., Edvardsson, D., Ekholuenetale, M., El Sayed, I., El-Jaafary, S. I., Eskandari, K., Eskandarieh, S., Esmaeilnejad, S., Fares, J., Faro, A., Farooque, U., Feigin, V. L., Feng, X., Fereshtehnejad, S.-M., Fernandes, E., Ferrara, P., Filip, I., Fillit, H., Fischer, F., Gaidhane, S., Galluzzo, L., Ghashghaee, A., Ghith, N., Gialluisi, A., Gilani, S. A., Glavan, I.-R., Gnedovskaya, E. V., Golechha, M., Gupta, R., Gupta, V. B., Gupta,

V. K., Haider, M. R., Hall, B. J., Hamidi, S., Hanif, A., Hankey, G. J., Haque, S., Hartono, R. K., Hasaballah, A. I., Hasan, M. T., Hassan, A., Hay, S. I., Hayat, K., Hegazy, M. I., Heidari, G., Heidari-Soureshjani, R., Herteliu, C., Househ, M., Hussain, R., Hwang, B.-F., Iacoviello, L., Iavicoli, I., Ilesanmi, O. S., Ilic, I. M., Ilic, M. D., Irvani, S. S. N., Iso, H., Iwagami, M., Jabbarinejad, R., Jacob, L., Jain, V., Jayapal, S. K., Jayawardena, R., Jha, R. P., Jonas, J. B., Joseph, N., Kalani, R., Kandel, A., Kandel, H., Karch, A., Kasa, A. S., Kassie, G. M., Keshavarz, P., Khan, M. A. B., Khatib, M. N., Khoja, T. A. M., Khubchandani, J., Kim, M. S., Kim, Y. J., Kisa, A., Kisa, S., Kivimäki, M., Koroshetz, W. J., Koyanagi, A., Kumar, G. A., Kumar, M., Lak, H. M., Leonardi, M., Li, B., Lim, S. S., Liu, X., Liu, Y., Logroscino, G., Lorkowski, S., Lucchetti, G., Lutzky Saute, R., Magnani, F. G., Malik, A. A., Massano, J., Mehndiratta, M. M., Menezes, R. G., Meretoja, A., Mohajer, B., Mohamed Ibrahim, N., Mohammad, Y., Mohammed, A., Mokdad, A. H., Mondello, S., Moni, M. A. A., Moniruzzaman, M., Mossie, T. B., Nagel, G., Naveed, M., Nayak, V. C., Neupane Kandel, S., Nguyen, T. H., Oancea, B., Otstavnov, N., Otstavnov, S. S., Owolabi, M. O., Panda-Jonas, S., Pashazadeh Kan, F., Pasovic, M., Patel, U. K., Pathak, M., Peres, M. F. P., Perianayagam, A., Peterson, C. B., Phillips, M. R., Pinheiro, M., Piradov, M. A., Pond, C. D., Potashman, M. H., Pottoo, F. H., Prada, S. I., Radfar, A., Raggi, A., Rahim, F., Rahman, M., Ram, P., Ranasinghe, P., Rawaf, D. L., Rawaf, S., Rezaei, N., Rezapour, A., Robinson, S. R., Romoli, M., Roshandel, G., Sahathevan, R., Sahebkar, A., Sahraian, M. A., Sathian, B., Sattin, D., Sawhney, M., Saylan, M., Schiavolin, S., Seylani, A., Sha, F., Shaikh, M. A., Shaji, K. S., Shannawaz, M., Shetty, J. K., Shigematsu, M., Shin, J. I., Shiri, R., Silva, D. A. S., Silva, J. P., Silva, R., Singh, J. A., Skryabin, V. Y., Skryabina, A. A., Smith, A. E., Soshnikov, S., Spurlock, E. E., Stein, D. J., Sun, J., Tabarés-Seisdedos, R., Thakur, B., Timalsina, B., Tovani-Palone, M. R., Tran, B. X., Tsegaye, G. W., Valadan Tahbaz, S., Valdez, P. R., Venketasubramanian, N., Vlassov, V., Vu, G. T., Vu, L. G., Wang, Y.-P., Wimo, A., Winkler, A. S., Yadav, L., Yahyazadeh Jabbari, S. H., Yamagishi, K., Yang, L., Yano, Y., Yonemoto, N., Yu, C., Yunusa, I., Zadey, S., Zastrozhin, M. S., Zastrozhina, A., Zhang, Z.-J., Murray, C. J. L., & Vos, T. (2022). Estimation of the global prevalence of dementia in 2019 and forecasted prevalence in 2050: an analysis for the Global Burden of Disease Study 2019. *The Lancet Public Health*, *7*(2), e105-e125. https://doi.org/10.1016/S2468-2667(21)00249-8

Nikoletopoulou, V., & Tavernarakis, N. (2012). Calcium homeostasis in aging neurons [Review]. *Frontiers in Genetics*, *Volume 3 - 2012*. https://doi.org/10.3389/fgene.2012.00200

Noebels, J. (2011). A perfect storm: Converging paths of epilepsy and Alzheimer's dementia intersect in the hippocampal formation. *Epilepsia*, *52 Suppl 1*(Suppl 1), 39-46. https://doi.org/10.1111/j.1528-1167.2010.02909.x

Palladino, M. J., Hadley, T. J., & Ganetzky, B. (2002). Temperature-sensitive paralytic mutants are enriched for those causing neurodegeneration in Drosophila. *Genetics*, *161*(3), 1197-1208. https://doi.org/10.1093/genetics/161.3.1197

Park, J.-H., Park, I., Youm, E. M., Lee, S., Park, J.-H., Lee, J., Lee, D. Y., Byun, M. S., Lee, J. H., Yi, D., Chung, S. J., Park, K. W., Choi, N., Kim, S. Y., Yoon, W., An,

H., Kim, K. w., Choi, S. H., Jeong, J. H., Kim, E.-J., Kang, H., Lee, J., Kim, Y., Lee, E. A., Seo, S. W., Na, D. L., & Kim, J.-W. (2021). Novel Alzheimer's disease risk variants identified based on whole-genome sequencing of APOE ε4 carriers. *Translational Psychiatry*, *11*(1), 296. https://doi.org/10.1038/s41398-021-01412-9

Pchitskaya, E., Popugaeva, E., & Bezprozvanny, I. (2018). Calcium signaling and molecular mechanisms underlying neurodegenerative diseases. *Cell Calcium*, *70*, 87-94. https://doi.org/https://doi.org/10.1016/j.ceca.2017.06.008

Peña-Bautista, C., Casas-Fernández, E., Vento, M., Baquero, M., & Cháfer-Pericás, C. (2020). Stress and neurodegeneration. *Clin Chim Acta*, *503*, 163-168. https://doi.org/10.1016/j.cca.2020.01.019

Pizzo, P., Drago, I., Filadi, R., & Pozzan, T. (2012). Mitochondrial Ca2+ homeostasis: mechanism, role, and tissue specificities. *Pflügers Archiv - European Journal of Physiology*, *464*(1), 3-17. https://doi.org/10.1007/s00424-012-1122-y

Pratt, J., De Vito, G., Narici, M., & Boreham, C. (2021). Neuromuscular Junction Aging: A Role for Biomarkers and Exercise. *J Gerontol A Biol Sci Med Sci*, *76*(4), 576-585. https://doi.org/10.1093/gerona/glaa207

Purushotham, M., Tashrifwala, F., Jena, R., Vudugula, S. A., Patil, R. S., & Agrawal, A. (2022). The Association Between Alzheimer's Disease and Epilepsy: A Narrative Review. *Cureus*, *14*(10), e30195. https://doi.org/10.7759/cureus.30195

Rossetto, M. G., Zanarella, E., Orso, G., Scorzeto, M., Megighian, A., Kumar, V., Delgado-Escueta, A. V., & Daga, A. (2011). Defhc1.1, a homologue of the juvenile myoclonic gene EFHC1, modulates architecture and basal activity of the neuromuscular junction in Drosophila. *Hum Mol Genet*, *20*(21), 4248-4257. https://doi.org/10.1093/hmg/ddr352

Schnetkamp, P. P. (2013). The SLC24 gene family of Na^+/Ca^{2+}-K^+ exchangers: from sight and smell to memory consolidation and skin pigmentation. *Mol Aspects Med*, *34*(2-3), 455-464. https://doi.org/10.1016/j.mam.2012.07.008

Sidisky, J. M., & Babcock, D. T. (2020). Visualizing Synaptic Degeneration in Adult Drosophila in Association with Neurodegeneration. *J Vis Exp*(159). https://doi.org/10.3791/61363

Sidisky, J. M., Weaver, D., Hussain, S., Okumus, M., Caratenuto, R., & Babcock, D. (2021). Mayday sustains trans-synaptic BMP signaling required for synaptic maintenance with age. *Elife*, *10*. https://doi.org/10.7554/eLife.54932

Stafstrom, C. E., & Carmant, L. (2015). Seizures and epilepsy: an overview for neuroscientists. *Cold Spring Harb Perspect Med*, *5*(6). https://doi.org/10.1101/cshperspect.a022426

Stolwijk, J. A., Zhang, X., Gueguinou, M., Zhang, W., Matrougui, K., Renken, C., & Trebak, M. (2016). Calcium Signaling Is Dispensable for Receptor Regulation of Endothelial Barrier Function. *J Biol Chem*, *291*(44), 22894-22912. https://doi.org/10.1074/jbc.M116.756114

Sun, D., Amiri, M., Meng, Q., Unnithan, R. R., & French, C. (2024). Calcium Signalling in Neurological Disorders, with Insights from Miniature Fluorescence Microscopy. *Cells*, *14*(1). https://doi.org/10.3390/cells14010004

Suzuki, D. T., Grigliatti, T., & Williamson, R. (1971). Temperature-sensitive mutations in Drosophila melanogaster, VII. A mutation (parats) causing reversible adult paralysis. *Proceedings of the National Academy of Sciences*, *68*(5), 890-893.

Suzuki, D. T., Grigliatti, T., & Williamson, R. (1971). Temperature-sensitive mutations in Drosophila melanogaster. VII. A mutation (para-ts) causing reversible adult paralysis. *Proc Natl Acad Sci U S A*, *68*(5), 890-893. https://doi.org/10.1073/pnas.68.5.890

Tombini, M., Assenza, G., Ricci, L., Lanzone, J., Boscarino, M., Vico, C., Magliozzi, A., & Di Lazzaro, V. (2021). Temporal Lobe Epilepsy and Alzheimer's Disease: From Preclinical to Clinical Evidence of a Strong Association. *J Alzheimers Dis Rep*, *5*(1), 243-261. https://doi.org/10.3233/adr-200286

von Stockum, S., Basso, E., Petronilli, V., Sabatelli, P., Forte, M. A., & Bernardi, P. (2011). Properties of Ca(2+) transport in mitochondria of Drosophila melanogaster. *J Biol Chem*, *286*(48), 41163-41170. https://doi.org/10.1074/jbc.M111.268375

Vonhoff, F., & Keshishian, H. (2017). In Vivo Calcium Signaling during Synaptic Refinement at the Drosophila Neuromuscular Junction. *J Neurosci*, *37*(22), 5511-5526. https://doi.org/10.1523/jneurosci.2922-16.2017

Wang, M., Zhang, H., Liang, J., Huang, J., Wu, T., & Chen, N. (2025). Calcium signaling hypothesis: A non-negligible pathogenesis in Alzheimer's disease. *J Adv Res*. https://doi.org/10.1016/j.jare.2025.01.007

Wang, P., Saraswati, S., Guan, Z., Watkins, C. J., Wurtman, R. J., & Littleton, J. T. (2004). A Drosophila temperature-sensitive seizure mutant in phosphoglycerate kinase disrupts ATP generation and alters synaptic function. *J Neurosci*, *24*(19), 4518-4529. https://doi.org/10.1523/jneurosci.0542-04.2004

Wang, Y., Moussian, B., Schaeffeler, E., Schwab, M., & Nies, A. T. (2018). The fruit fly Drosophila melanogaster as an innovative preclinical ADME model for solute carrier membrane transporters, with consequences for pharmacology and drug therapy. *Drug Discovery Today*, *23*(10), 1746-1760. https://doi.org/https://doi.org/10.1016/j.drudis.2018.06.002

Webel, R., Haug-Collet, K., Pearson, B., Szerencsei, R. T., Winkfein, R. J., Schnetkamp, P. P., & Colley, N. J. (2002). Potassium-dependent sodium-calcium exchange through the eye of the fly. *Ann N Y Acad Sci*, *976*, 300-314. https://doi.org/10.1111/j.1749-6632.2002.tb04753.x

Winkfein, R. J., Pearson, B., Ward, R., Szerencsei, R. T., Colley, N. J., & Schnetkamp, P. P. (2004). Molecular characterization, functional expression and tissue distribution of a second NCKX Na+/Ca2+ -K+ exchanger from Drosophila. *Cell Calcium*, *36*(2), 147-155. https://doi.org/10.1016/j.ceca.2004.01.021

Winkfein, R. J., Szerencsei, R. T., Kinjo, T. G., Kang, Perizzolo, M., Eisner, L., & Schnetkamp, P. P. M. (2003). Scanning Mutagenesis of the Alpha Repeats and of the Transmembrane Acidic Residues of the Human Retinal Cone Na/Ca-K Exchanger. *Biochemistry*, *42*(2), 543-552. https://doi.org/10.1021/bi026982x

Xie, W., Koppula, S., Kale, M. B., Ali, L. S., Wankhede, N. L., Umare, M. D., Upaganlawar, A. B., Abdeen, A., Ebrahim, E. E., & El-Sherbiny, M. (2024). Unraveling the nexus of age, epilepsy, and mitochondria: exploring the dynamics of cellular energy and excitability. *Frontiers in Pharmacology*, *15*, 1469053.

Zhang, Y., Sharma, S., & Lytton, J. (2015). Anatomical evidence for a non-synaptic influence of the K+ -dependent Na+/Ca2+ -exchanger, NCKX2, on hippocampal

plasticity. *Neuroscience*, *310*, 372-388. https://doi.org/10.1016/j.neuroscience.2015.09.049

Zhou, X., Chen, Z., Xiao, L., Zhong, Y., Liu, Y., Wu, J., & Tao, H. (2022). Intracellular calcium homeostasis and its dysregulation underlying epileptic seizures. *Seizure*, *103*, 126-136. https://doi.org/10.1016/j.seizure.2022.11.007

Figure 1

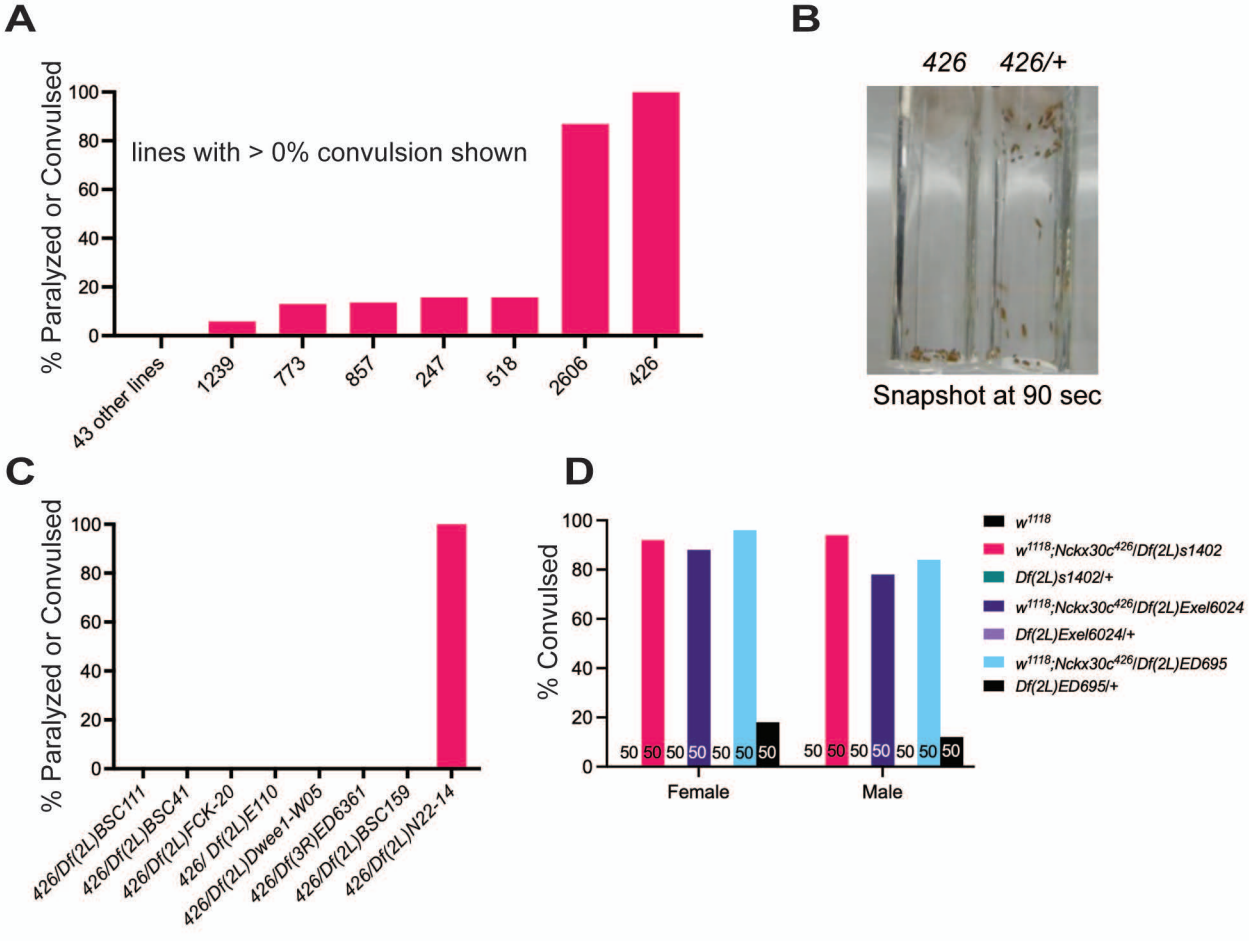
A
% Paralyzed or Convulsed
100
80
60
40
20
0
lines with > 0% convulsion shown
43 other lines
1239
773
857
247
518
2606
426
B
426
426/+
Snapshot at 90 sec
C
% Paralyzed or Convulsed
100
80
60
40
20
0
426/Df(2L)BSC111
426/Df(2L)BSC41
426/Df(2L)FCK-20
426/ Df(2L)E110
426/Df(2L)Dwee1-W05
426/Df(3R)ED6361
426/Df(2L)BSC159
426/Df(2L)N22-14
D
% Convulsed
100
80
60
40
20
0
50
Female
Male
w1118
w1118;Nckx30c426/Df(2L)s1402
Df(2L)s1402/+
w1118;Nckx30c426/Df(2L)Exel6024
Df(2L)Exel6024/+
w1118;Nckx30c426/Df(2L)ED695
Df(2L)ED695/+

Figure 2

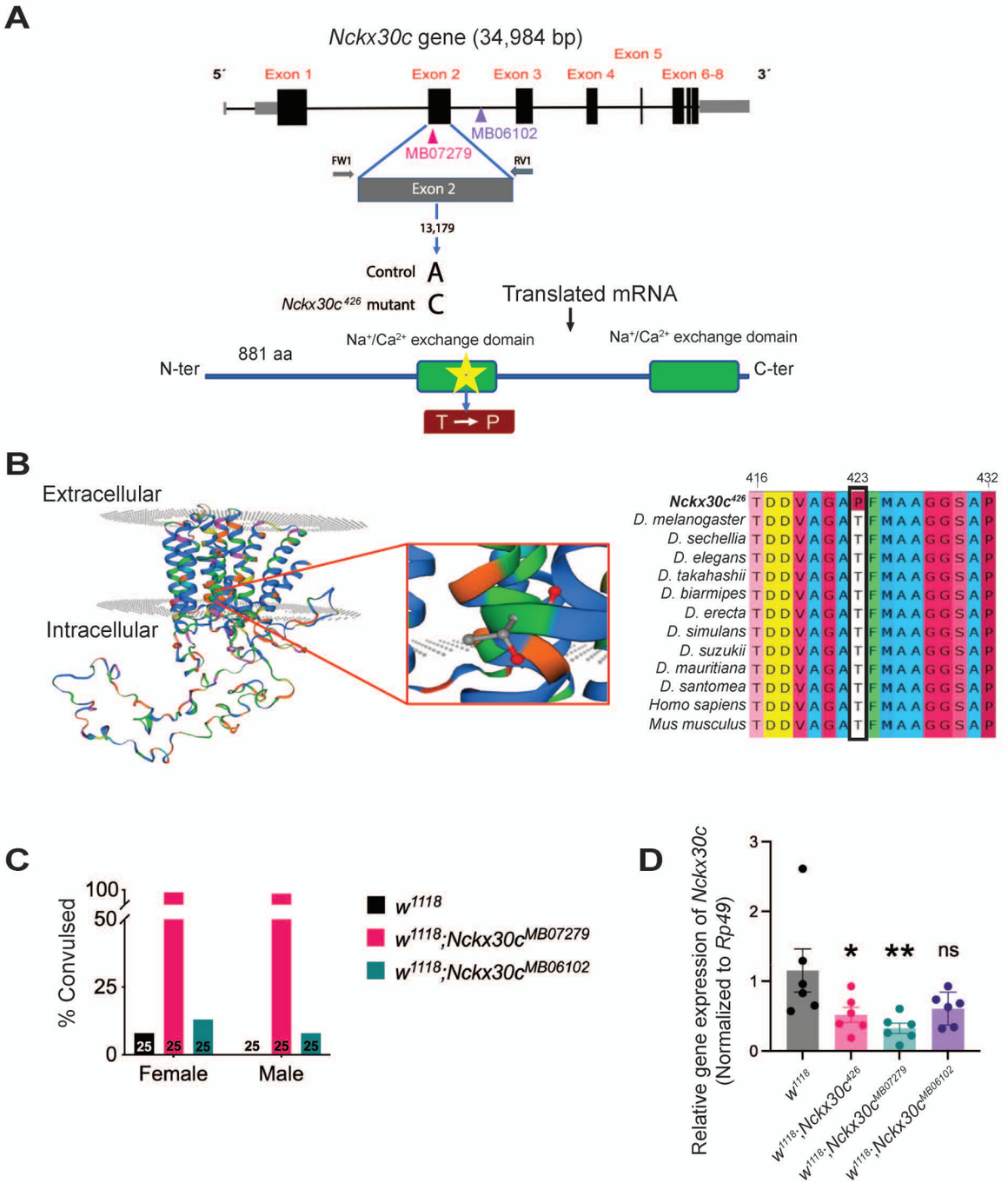
A
Nckx30c gene (34,984 bp)
5´
Exon 1
Exon 2
Exon 3
Exon 4
Exon 5
Exon 6-8
3´
MB06102
MB07279
FW1
RV1
Exon 2
13,179
Control A
Nckx30c426 mutant C
Translated mRNA
Na+/Ca2+ exchange domain
Na+/Ca2+ exchange domain
N-ter
881 aa
C-ter
T → P
B
Extracellular
Intracellular
416
423
432
Nckx30c426 T D D V A G A P F M A A G G S A P
D. melanogaster T D D V A G A T F M A A G G S A P
D. sechellia T D D V A G A T F M A A G G S A P
D. elegans T D D V A G A T F M A A G G S A P
D. takahashii T D D V A G A T F M A A G G S A P
D. biarmipes T D D V A G A T F M A A G G S A P
D. erecta T D D V A G A T F M A A G G S A P
D. simulans T D D V A G A T F M A A G G S A P
D. suzukii T D D V A G A T F M A A G G S A P
D. mauritiana T D D V A G A T F M A A G G S A P
D. santomea T D D V A G A T F M A A G G S A P
Homo sapiens T D D V A G A T F M A A G G S A P
Mus musculus T D D V A G A T F M A A G G S A P
C
% Convulsed
100
50
25
0
25
25
25
25
25
25
Female
Male
w1118
w1118;Nckx30cMB07279
w1118;Nckx30cMB06102
D
Relative gene expression of Nckx30c
(Normalized to Rp49)
3
2
1
0
*
**
ns
w1118
w1118;Nckx30c426
w1118;Nckx30cMB07279
w1118;Nckx30cMB06102

Figure 3

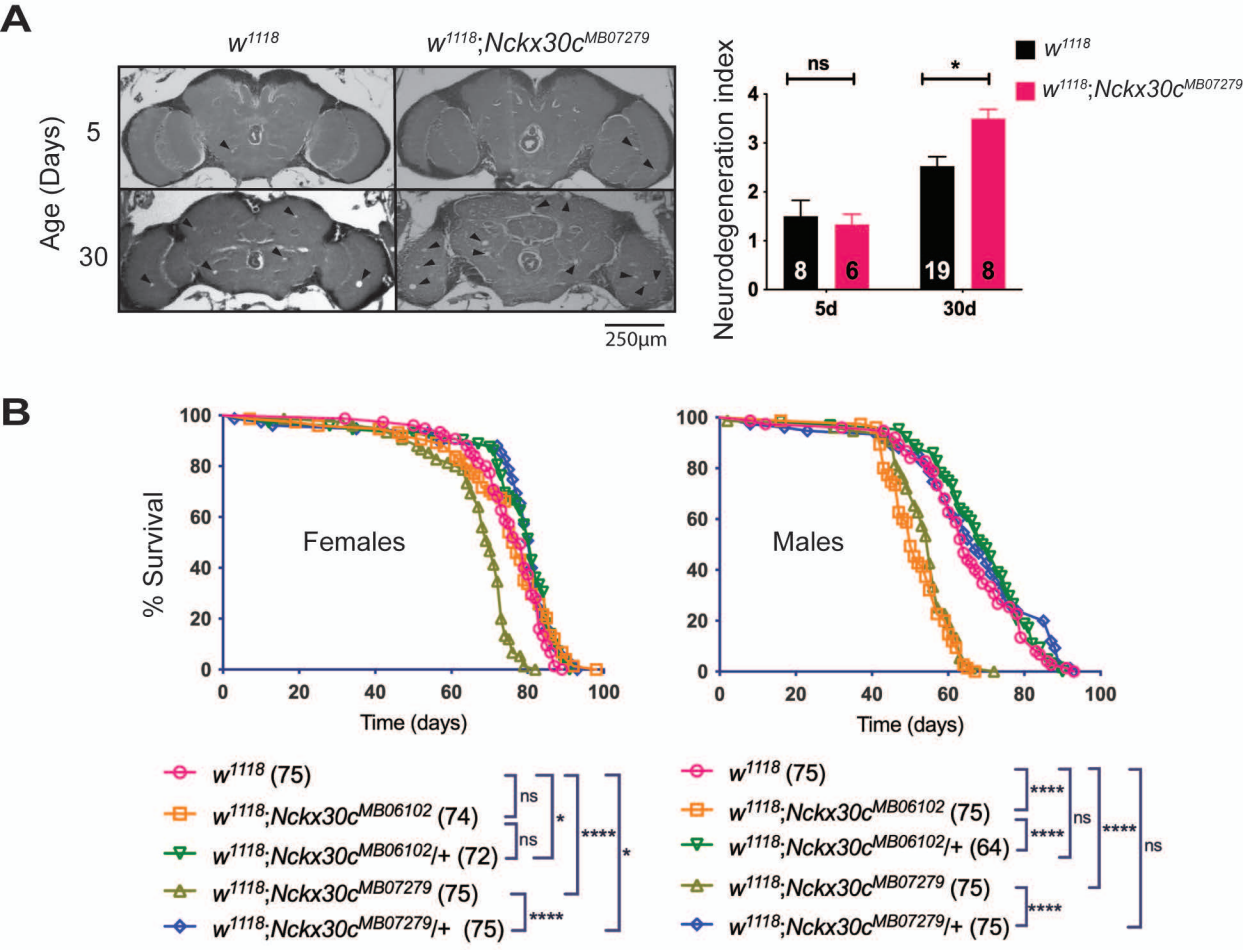
A
w1118
w1118;Nckx30cMB07279
Age (Days)
5
30
250µm
Neurodegeneration index
ns
*
w1118
w1118;Nckx30cMB07279
8
6
19
8
5d
30d
B
% Survival
Females
Males
Time (days)
w1118 (75)
w1118;Nckx30cMB06102 (74)
w1118;Nckx30cMB06102/+ (72)
w1118;Nckx30cMB07279 (75)
w1118;Nckx30cMB07279/+ (75)
w1118 (75)
w1118;Nckx30cMB06102 (75)
w1118;Nckx30cMB06102/+ (64)
w1118;Nckx30cMB07279 (75)
w1118;Nckx30cMB07279/+ (75)
ns
*
****

Figure 4

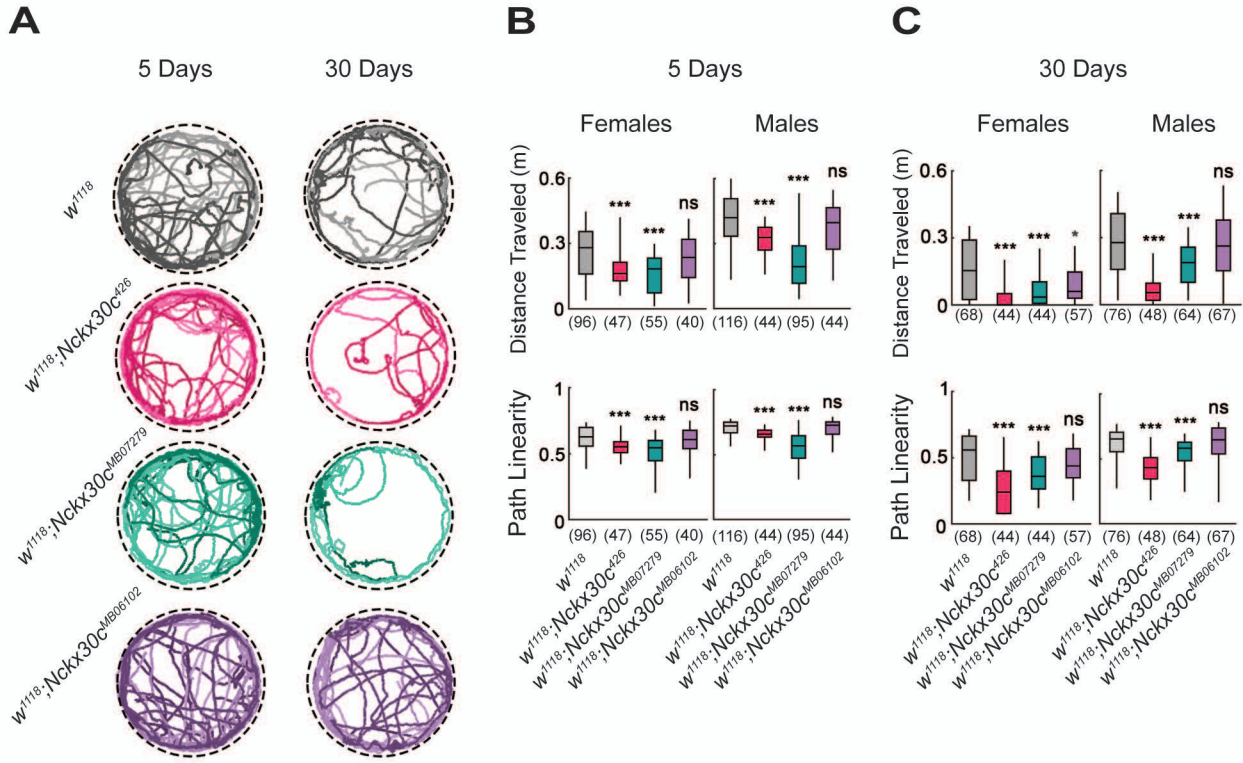
A
5 Days
30 Days
w1118
w1118;Nckx30c426
w1118;Nckx30cMB07279
w1118;Nckx30cMB06102
B
5 Days
Females
Males
Distance Traveled (m)
0.6
0.3
0
***
***
ns
***
***
ns
(96) (47) (55) (40)
(116) (44) (95) (44)
Path Linearity
1
0.5
0
***
***
ns
***
***
ns
(96) (47) (55) (40)
(116) (44) (95) (44)
w1118
w1118;Nckx30c426
w1118;Nckx30cMB07279
w1118;Nckx30cMB06102
w1118
w1118;Nckx30c426
w1118;Nckx30cMB07279
w1118;Nckx30cMB06102
C
30 Days
Females
Males
Distance Traveled (m)
0.6
0.3
0
***
***
*
ns
***
***
ns
(68) (44) (44) (57)
(76) (48) (64) (67)
Path Linearity
1
0.5
0
***
***
ns
***
***
ns
(68) (44) (44) (57)
(76) (48) (64) (67)
w1118
w1118;Nckx30c426
w1118;Nckx30cMB07279
w1118;Nckx30cMB06102
w1118
w1118;Nckx30c426
w1118;Nckx30cMB07279
w1118;Nckx30cMB06102

Figure 5

A

Larval NMJ (Muscle 4)

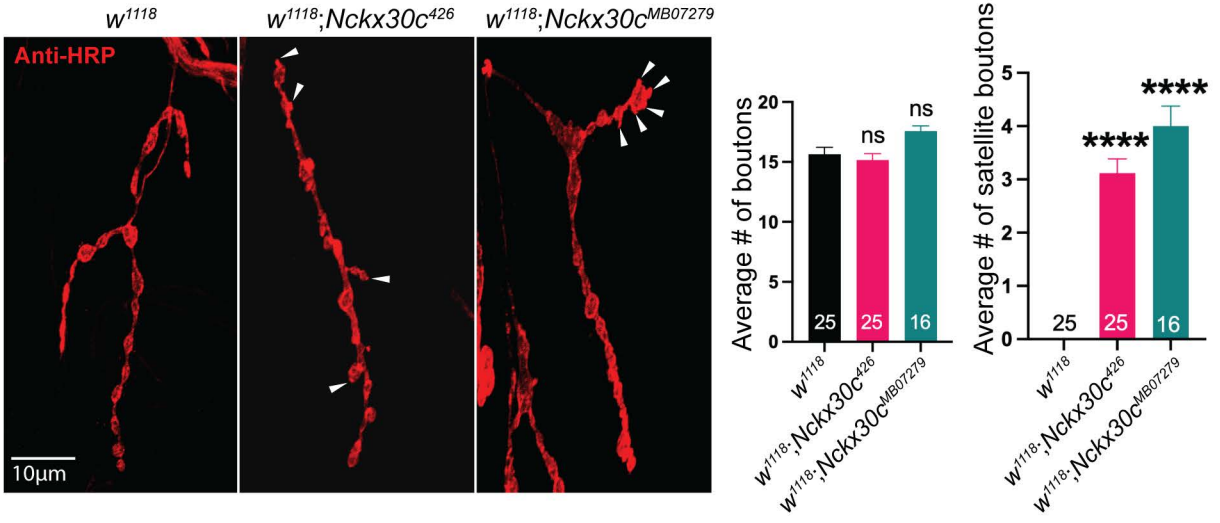

B

Adult DLM NMJ

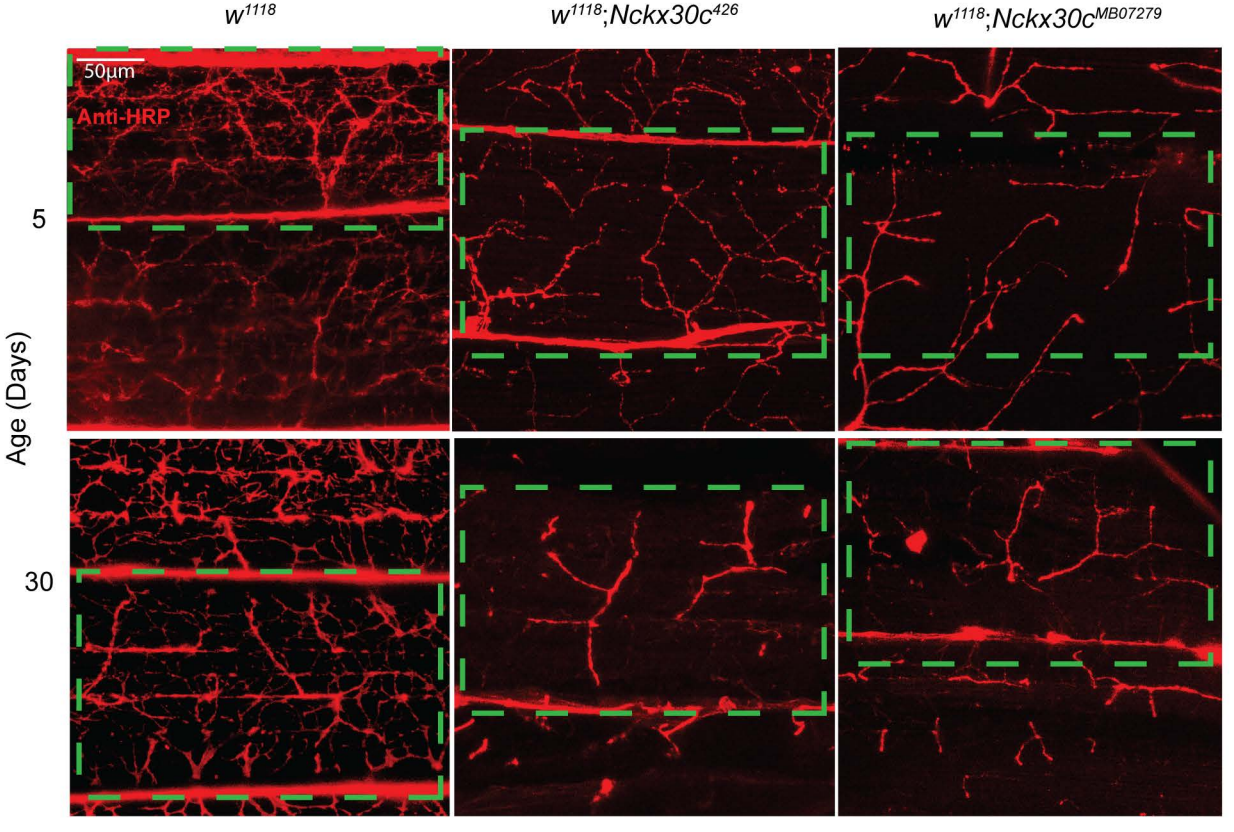

Figure 6

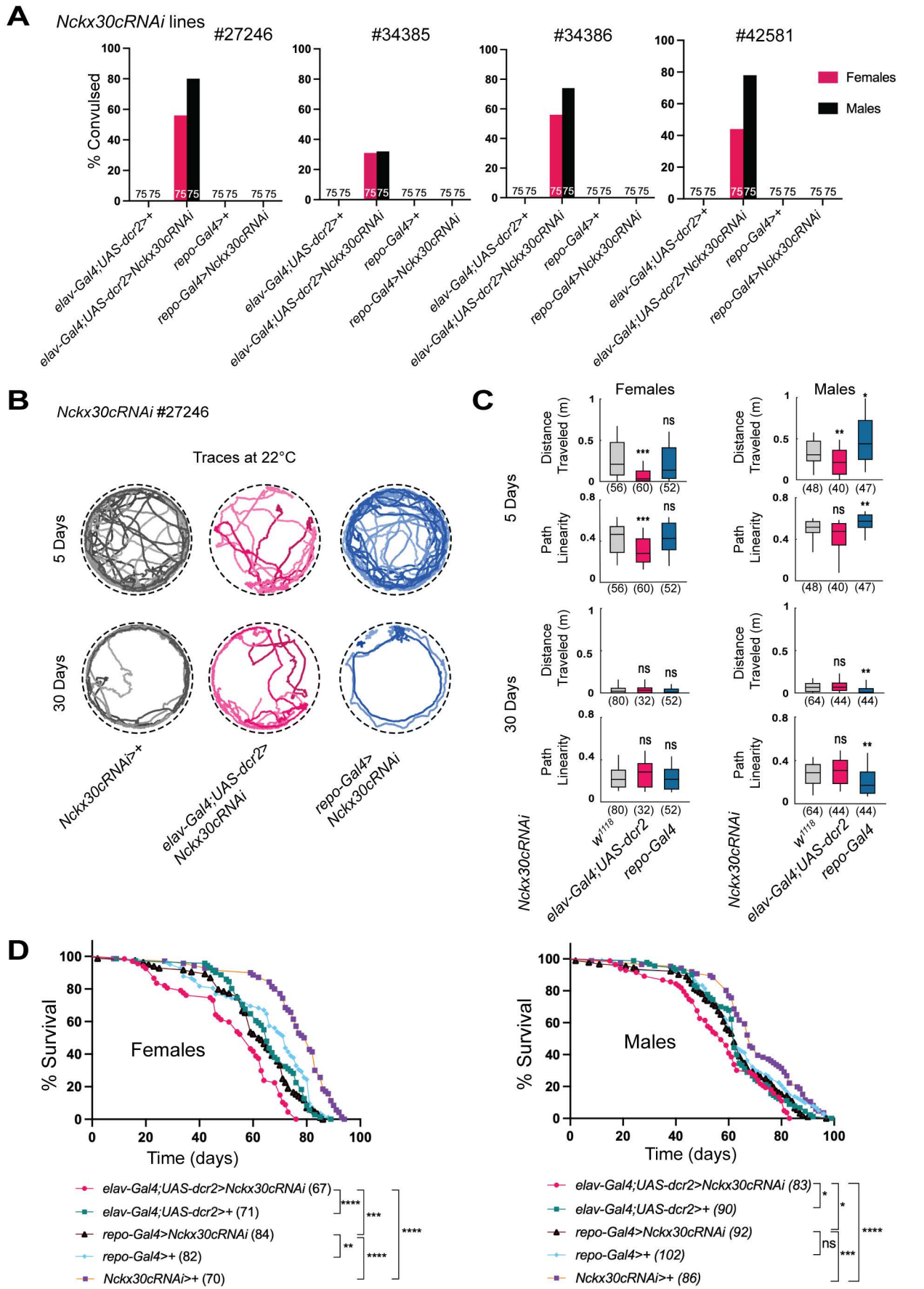
A
Nckx30cRNAi lines
#27246
#34385
#34386
#42581
% Convulsed
Females
Males
elav-Gal4;UAS-dcr2>+
elav-Gal4;UAS-dcr2>Nckx30cRNAi
repo-Gal4>+
repo-Gal4>Nckx30cRNAi
B
Nckx30cRNAi #27246
Traces at 22°C
5 Days
30 Days
Nckx30cRNAi>+
elav-Gal4;UAS-dcr2> Nckx30cRNAi
repo-Gal4> Nckx30cRNAi
C
Females
Males
Distance Traveled (m)
Path Linearity
5 Days
30 Days
w1118
elav-Gal4;UAS-dcr2
repo-Gal4
Nckx30cRNAi
D
% Survival
Time (days)
Females
Males
elav-Gal4;UAS-dcr2>Nckx30cRNAi (67)
elav-Gal4;UAS-dcr2>+ (71)
repo-Gal4>Nckx30cRNAi (84)
repo-Gal4>+ (82)
Nckx30cRNAi>+ (70)
elav-Gal4;UAS-dcr2>Nckx30cRNAi (83)
elav-Gal4;UAS-dcr2>+ (90)
repo-Gal4>Nckx30cRNAi (92)
repo-Gal4>+ (102)
Nckx30cRNAi>+ (86)

Figure S1

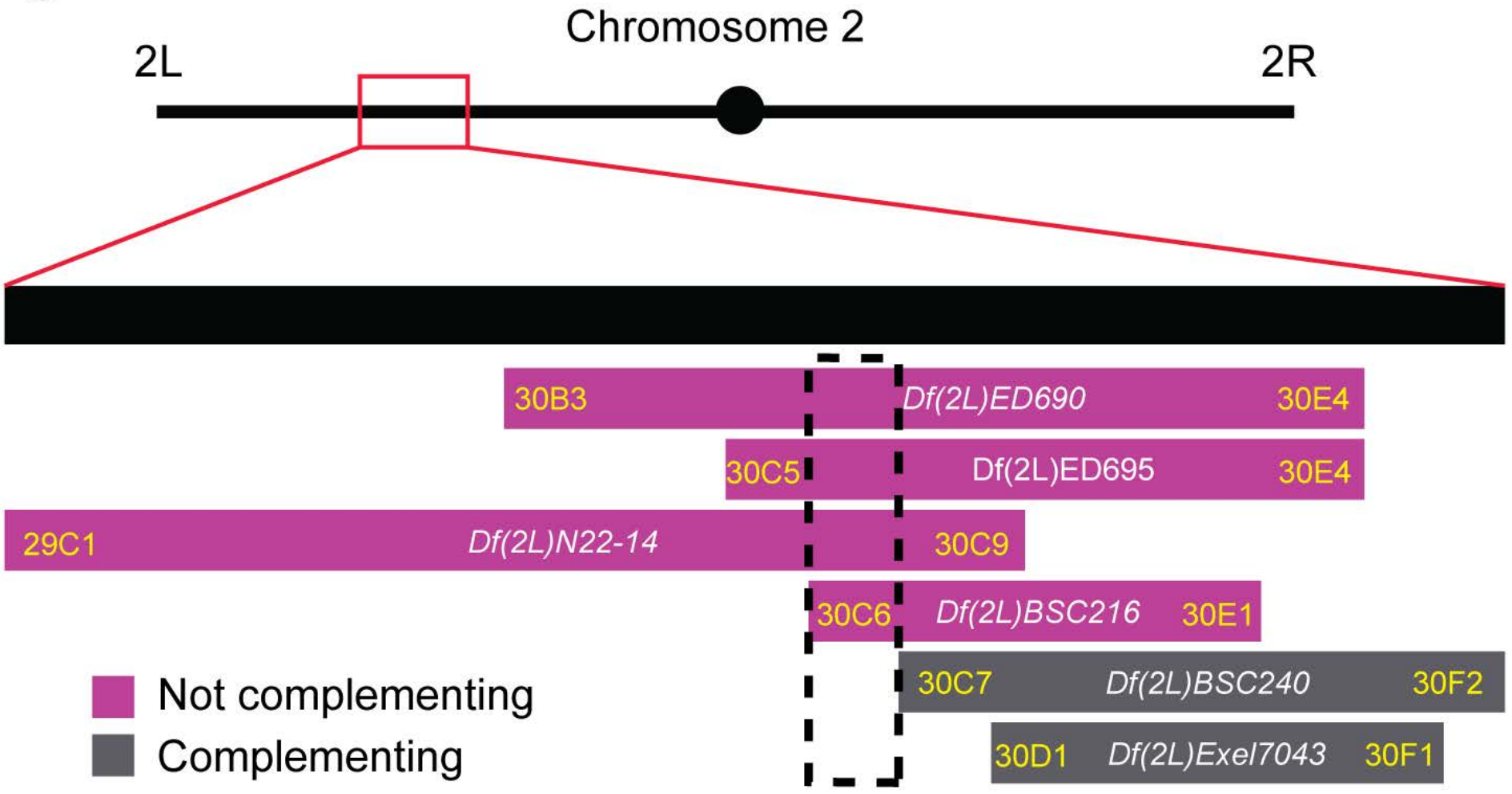
Chromosome 2
2L
2R
30B3
Df(2L)ED690
30E4
30C5
Df(2L)ED695
30E4
29C1
Df(2L)N22-14
30C9
30C6
Df(2L)BSC216
30E1
30C7
Df(2L)BSC240
30F2
30D1
Df(2L)Exel7043
30F1
Not complementing
Complementing

Figure S2

A

cDNA sequencing alignment

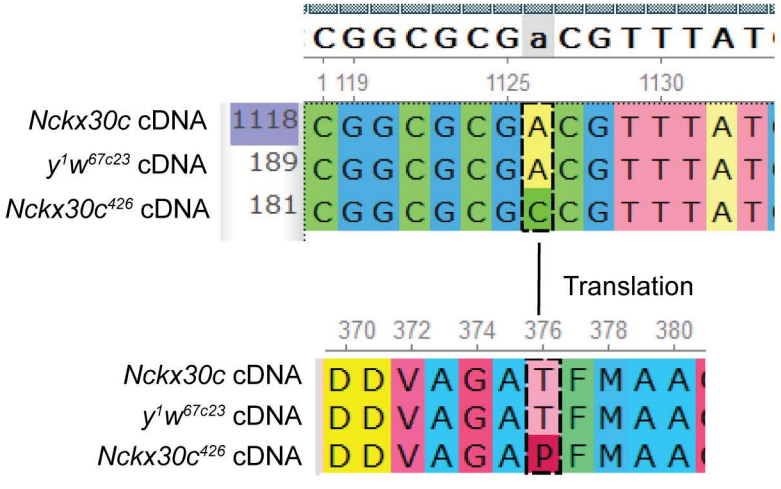

B

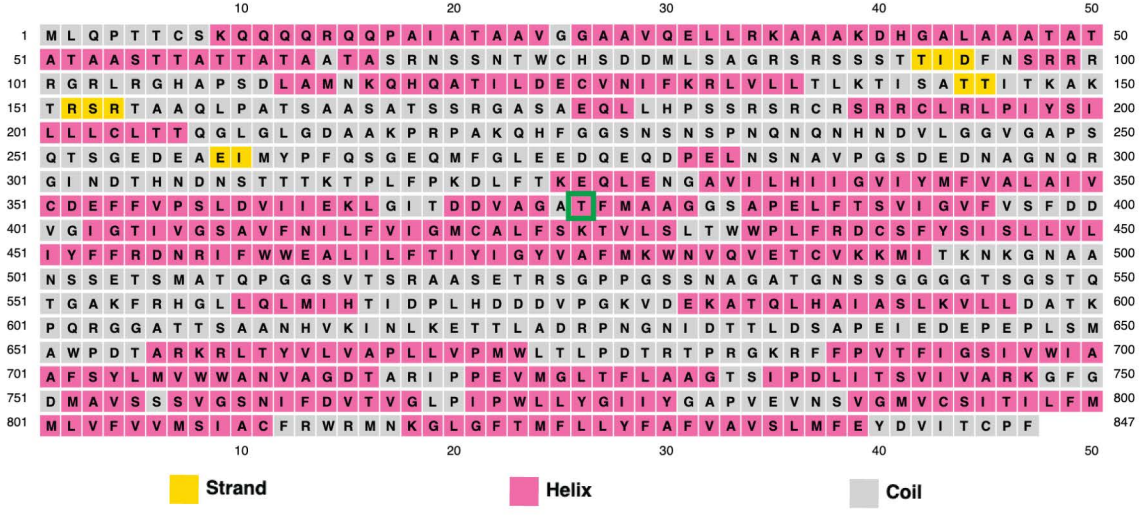

Figure S3

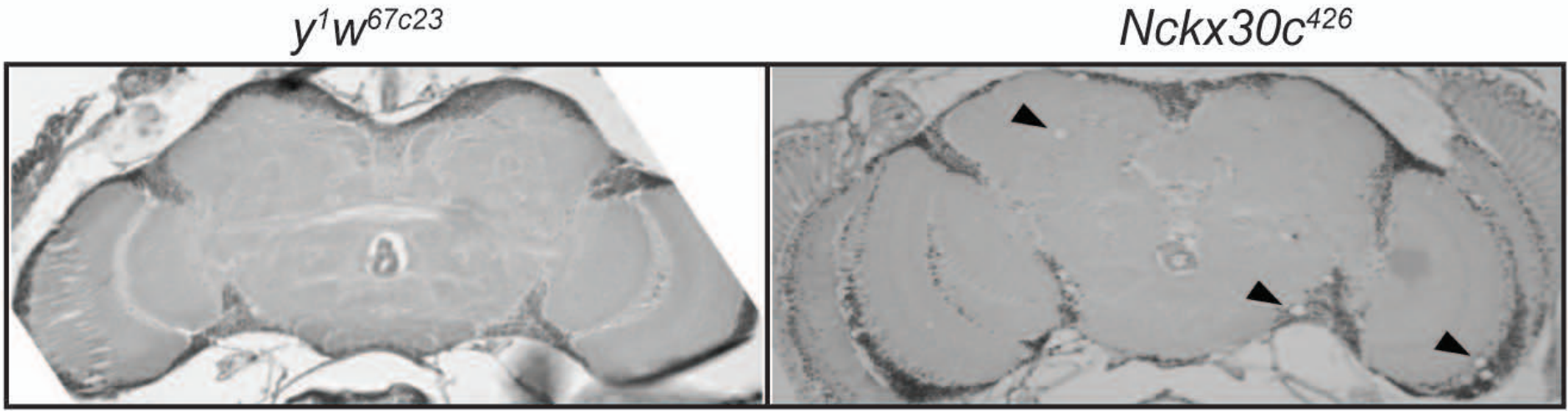

Figure S4

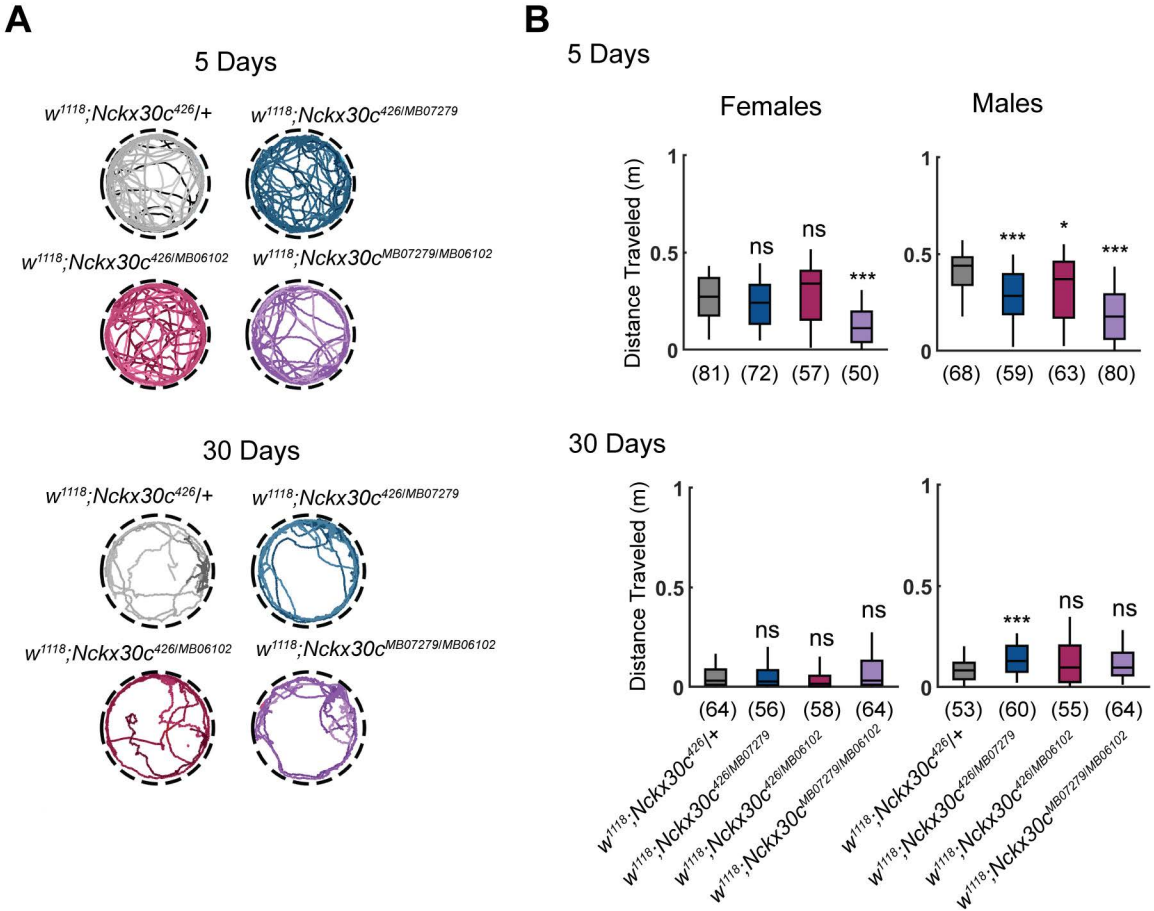
A
5 Days
w1118;Nckx30c426/+
w1118;Nckx30c426/MB07279
w1118;Nckx30c426/MB06102
w1118;Nckx30cMB07279/MB06102
30 Days
w1118;Nckx30c426/+
w1118;Nckx30c426/MB07279
w1118;Nckx30c426/MB06102
w1118;Nckx30cMB07279/MB06102
B
5 Days
Females
Males
Distance Traveled (m)
1
0.5
0
ns
ns
***
(81) (72) (57) (50)
***
*
***
(68) (59) (63) (80)
30 Days
Distance Traveled (m)
ns
ns
ns
(64) (56) (58) (64)
***
ns
ns
(53) (60) (55) (64)
w1118;Nckx30c426/+
w1118;Nckx30c426/MB07279
w1118;Nckx30c426/MB06102
w1118;Nckx30cMB07279/MB06102

Figure S5

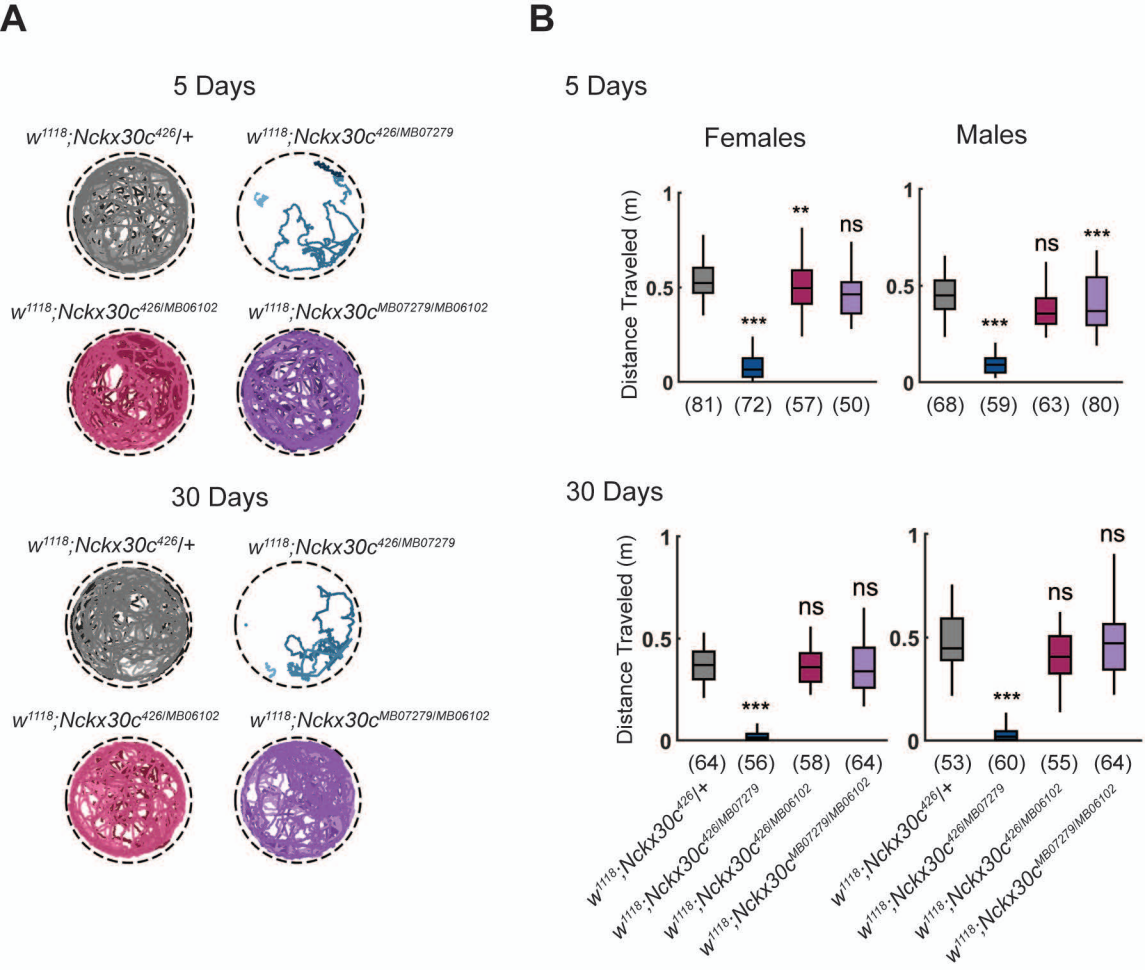
A
5 Days
w1118;Nckx30c426/+
w1118;Nckx30c426/MB07279
w1118;Nckx30c426/MB06102
w1118;NckxMB07279/MB06102
30 Days
w1118;Nckx30c426/+
w1118;Nckx30c426/MB07279
w1118;Nckx30c426/MB06102
w1118;NckxMB07279/MB06102
B
5 Days
Females
Males
Distance Traveled (m)
1
0.5
0
***
**
ns
(81) (72) (57) (50)
(68) (59) (63) (80)
30 Days
(64) (56) (58) (64)
(53) (60) (55) (64)
w1118;Nckx30c426/+
w1118;Nckx30c426/MB07279
w1118;Nckx30c426/MB06102
w1118;NckxMB07279/MB06102

Figure S6

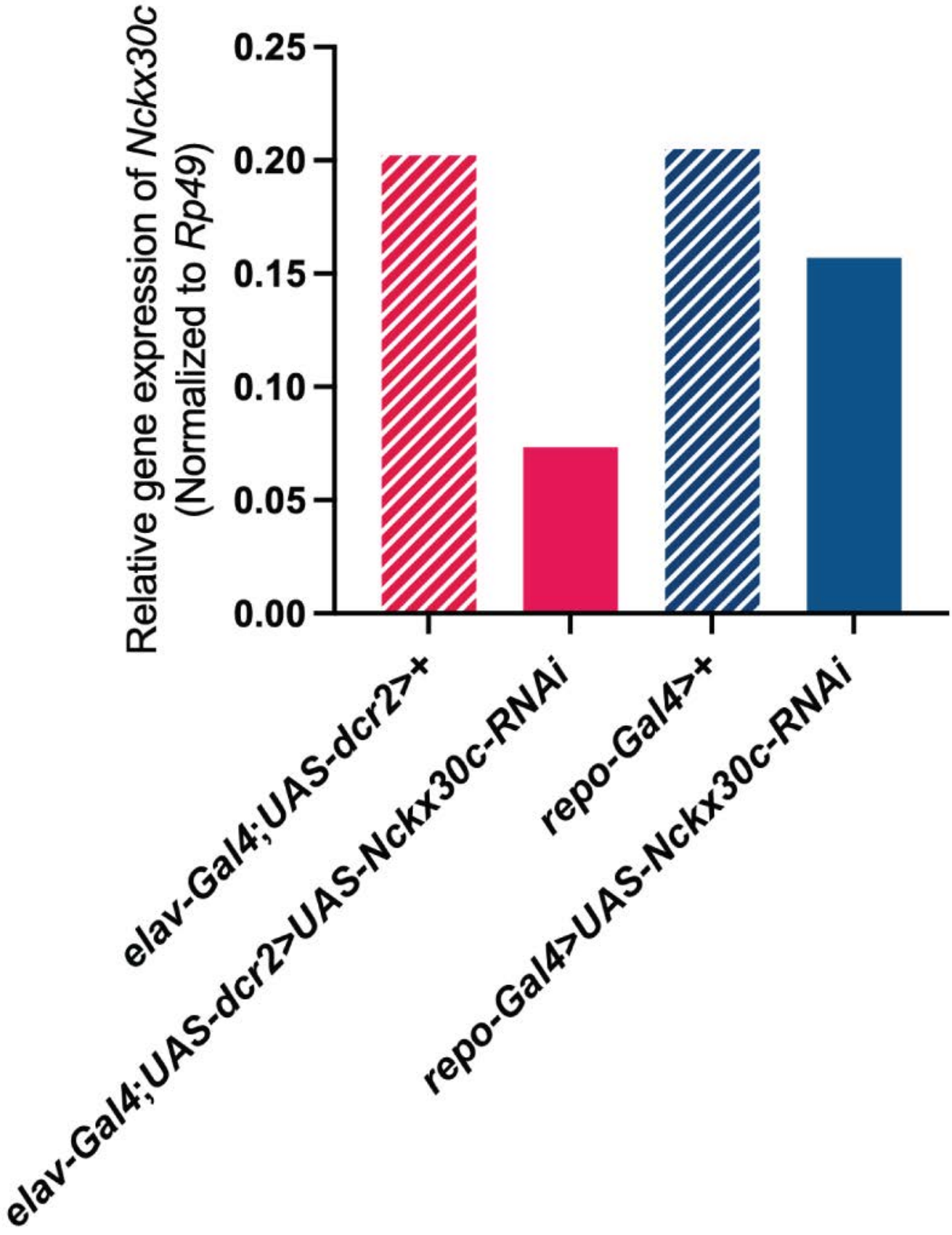
Relative gene expression of *Nckx30c*
(Normalized to *Rp49*)
0.25
0.20
0.15
0.10
0.05
0.00
elav-Gal4;UAS-dcr2>+
elav-Gal4;UAS-dcr2>UAS-Nckx30c-RNAi
repo-Gal4>+
repo-Gal4>UAS-Nckx30c-RNAi

Figure S7

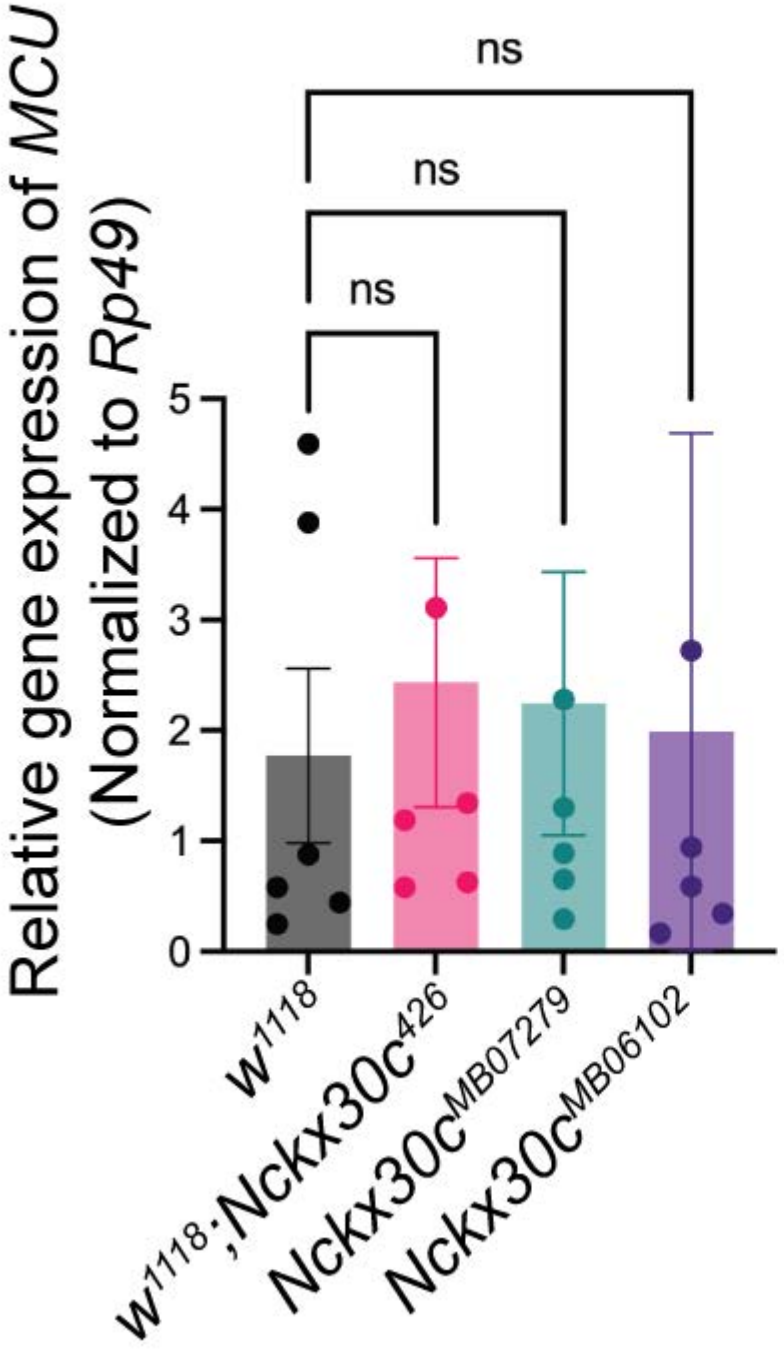
Relative gene expression of MCU
(Normalized to Rp49)
ns
ns
ns
5
4
3
2
1
0
w1118
w1118;Nckx30c426
Nckx30cMB07279
Nckx30cMB06102

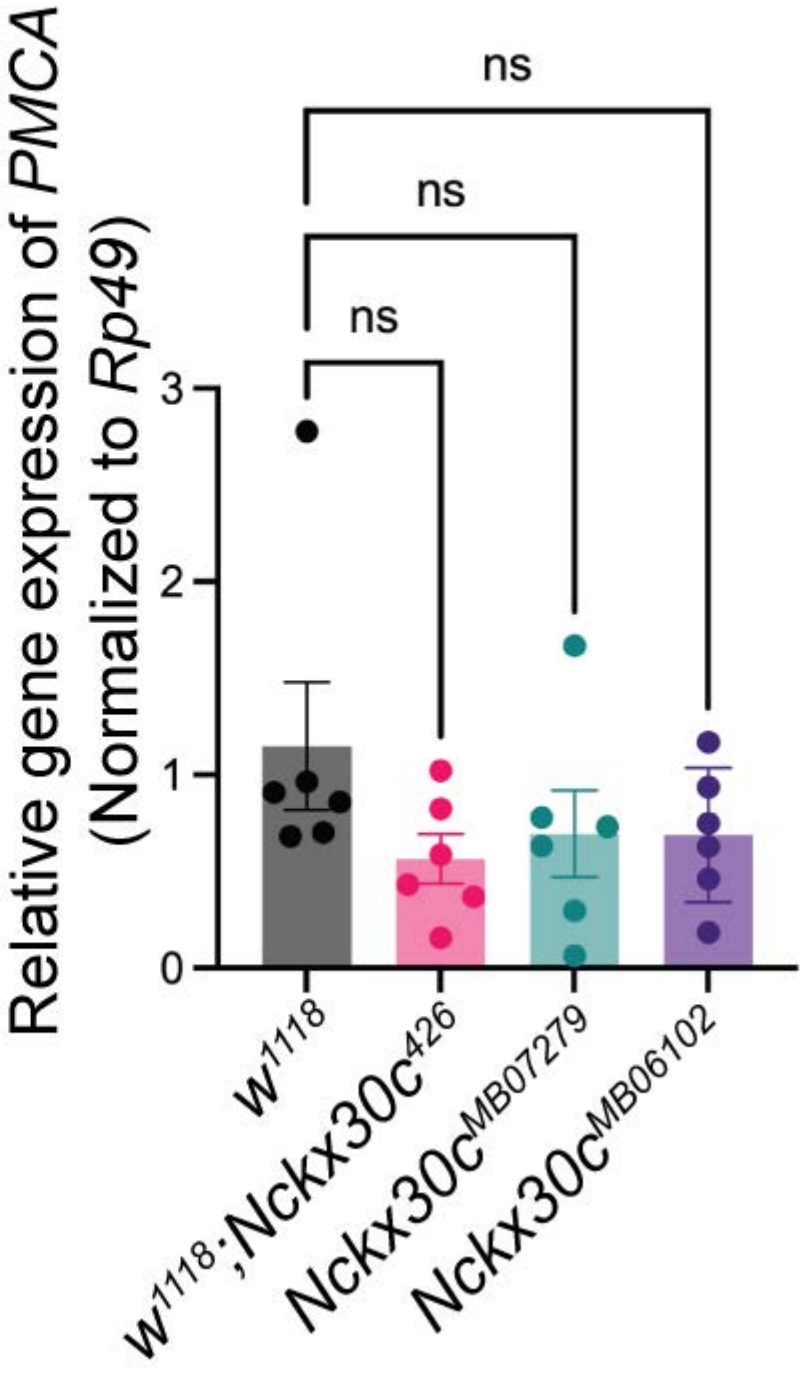
Relative gene expression of PMCA
(Normalized to Rp49)
ns
ns
ns
3
2
1
0
w1118
w1118;Nckx30c426
Nckx30cMB07279
Nckx30cMB06102

Supplementary Table 1: List of primers used in this study

Target name	Primer sequence
Exon 1 (PCR)	FW: 5' – *TGGCGTGAAAAATACCACAAGA – 3'* RV: 5' – CACGACGAACTGATTACCGT – 3'
Exon 2 (PCR)	FW: 5' – *GCGATGGAAAATTCCTCGAAAA – 3'* RV: 5' –CTCTTTCGCTTTAACTTTCGGT – 3'
Exon 3 (PCR)	FW: 5' – *CCGATAAACCCGATACCGAAAC – 3'* RV: 5' –*GGTCTCGAAGGGTTGGTGTTA* – 3'
Exon 4 (PCR)	FW: 5' – *CAACACCACCAACACCTCAC – 3'* RV: 5' –*GCTTGCCTAGACTTACAGCA* – 3'
Exon 5 (PCR)	FW: 5' – *TCTTTCCCGATCCGTATGTGT – 3'* RV: 5' –*CTTACGGGTCTTACAGTCCAA* – 3'
Exon 6 (PCR)	FW: 5' – *AGTTCGGTCCAAGTCGCTAA* – 3' RV: 5' –*CGTCTGGTTTAAGTAAGGGTCT* – 3'
Exon 7-8 (PCR)	FW: 5' – *ATTCCGCCCGAGGTACAATC* – 3' RV: 5' –*TCGGAGTGTGGGTTAATCGA* – 3'
Nckx30c cDNA pair 1	FW: 5' – ATTGCTCCACCCAAGTAGCC – 3' RV: 5' – GCCCACATCATCGAACGACACG – 3'
Nckx30c cDNA pair 2	FW: 5' – GCATTGGTACGATCGTTGGC – 3' RV: 5' – GGTGGTGTCGATGTTCCCAT – 3'
Nckx30c cDNA pair 3	FW: 5' – TAGTACTCAGACCGGTGCCA – 3' RV: 5' – GTGCCACAATCACCGAGGTA – 3'
Rp49 (RT-qPCR)	FW: 5' – AAGAAGCGCACCAAGCACTTCATC– 3' FW: 5' – TCTGTTGTCGATACCCTTGGGCTT– 3'
Nckx30c (RT-qPCR)	FW: 5' – ATGTTGCAGCCAACAACATG – 3' RV: 5' – TTAAAAGGGGCACGTGATCA – 3'
PMCA (RT-qPCR)	FW: 5' – GGTCGTGAGGGTGTAATGAAG– 3' RV: 5' – GTCAGCTTTCGATCCACTTAGG– 3'
MCU (RT-qPCR)	FW: 5' – ATGAGCTTCAGCAGCACAGA– 3' RV: 5' – CTTGAACTGTGACCTCCCGT– 3'